A versatile template for the formation of [2]pseudorotaxanes. 1,2-Bis(pyridinium)ethane axles and 24-crown-8 ether wheels†

Stephen J. Loeb,* Jorge Tiburcio, Sarah J. Vella and James A. Wisner

Received 13th October 2005, Accepted 25th November 2005
First published as an Advance Article on the web 6th January 2006
DOI: 10.1039/b514528g

Linear 1,2-bis(pyridinium)ethane 'axles' and macrocyclic 24-membered crown ether 'wheels' (**24C8**, **DB24C8** and **DN24C8**) combine to form [2]pseudorotaxanes. These interpenetrated adducts are held together by $N^+ \cdots O$ ion-dipole interactions, a series of C–H $\cdots$ O hydrogen bonds and π-stacking between electron-poor pyridinium rings of the axle and electron-rich catechol rings of the wheel. ^{1}H NMR spectroscopy was used to identify the structural details of the interaction and to determine the thermodynamics of the binding process in solution. Analysis of nine of these adducts by single crystal X-ray crystallography allowed a detailed study of the non-covalent interactions in the solid state. A wide variety of structural changes could be made to the system. The versatility and potential of the template for the construction of permanently interlocked structures such as rotaxanes and catenanes is discussed.

Introduction

A number of templating strategies now exist for the preparation of mechanically interlocked molecules such as rotaxanes and catenanes.[1] The most common synthetic methodology, 'threading' followed by 'stoppering', requires the identification of two components, a linear 'axle' and a cyclic 'wheel' that can interpenetrate and form a stable host–guest pair known as a [2]pseudorotaxane.[2] This can then be converted to a permanently interlocked rotaxane by capping with bulky groups or to a catenane by linking the two ends of the linear axle.[3]

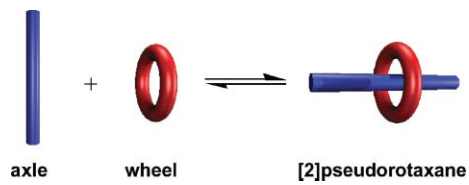

A wide array of complementary components capable of pseudorotaxane formation can be envisioned, but there still remains only a handful of chemical systems that are both efficient at threading and offer true flexibility for structural modification.[4] Indeed, it is these few versatile systems that have been exploited to create families of mechanically linked molecules and, by extension, molecular machines and devices.[5]

We have reported in a preliminary communication that linear 1,2-bis(pyridinium)ethane 'axles' and macrocyclic 24-membered crown ether 'wheels' can combine to form [2]pseudorotaxanes.[6] These interpenetrated adducts are held together by $N^+ \cdots O$ ion-dipole interactions, a series of C–H $\cdots$ O hydrogen bonds and in some cases π-stacking between the electron-poor pyridinium rings of the axle and electron-rich catechol rings appended to the wheel.

Although there are some superficial similarities to both the paraquat⊂BPP34C10[7] (bis-paraphenylene-34-crown-10) and secondary ammonium ion⊂24-crown-8 ether[8] systems in terms of the interactions involved, this system has some unique aspects and has shown to be extremely versatile in the breadth of structural changes that can be imposed without destruction of the basic templating interaction. To date, we have fashioned various rotaxanes,[9] catenanes,[10] molecular shuttles[11] and other molecular machines[12] as well as a variety of polyrotaxanes[13] employing this motif. Herein, we present a detailed study of the physical properties and structural features of this [2]pseudorotaxane templating motif. Scheme 1 outlines the variety of axles and crowns explored in this study. We have focused on systematically varying substituents on both the axle and wheel.

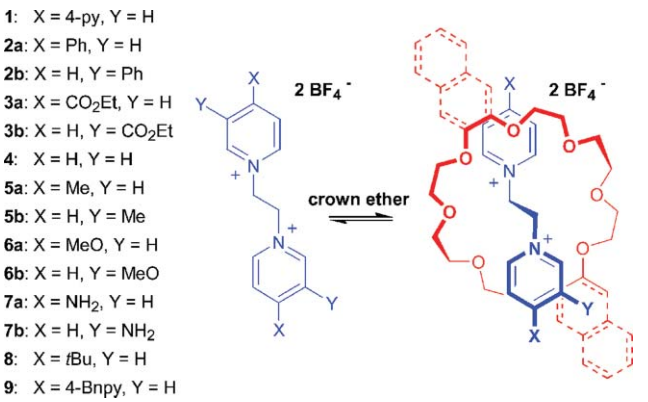

Scheme 1 Listing of the 1,2-bis(pyridinium)ethane axles investigated in this study and their reaction with 24-membered crown ethers, **24C8**, **DB24C8** and **DN24C8** to form [2]pseudorotaxanes.

Department of Chemistry and Biochemistry, University of Windsor, Windsor, ON, Canada N9B 3P4. E-mail: loeb@uwindsor.ca; Fax: 1-519-973-7098; Tel: 1-519-253-3000

† Electronic supplementary information (ESI) available: Van't Hoff plots, titrations and Hammett plots for [2]pseudorotaxanes involving **24C8**, **DB24C8** and **DN24C8**. See DOI: 10.1039/b514528g

Results and discussion

The 1,2-bis(pyridinium)ethane salts are easily synthesized[14] from the reaction between an excess of the corresponding pyridine and 1,2-dibromoethane in refluxing acetonitrile. These reactions render the axles as the bromide salts, which can be easily transformed into the corresponding tetrafluoroborate salts by anion exchange. This increases their solubility in polar organic solvents such as MeCN or $MeNO_2$ and importantly leads to a situation with essentially no ion pairing in solution.[15]

The mixing of any of the 1,2-bis(pyridinium)ethane axles, $\mathbf{1}^{2+}$–$\mathbf{7}^{2+}$ or $\mathbf{9}^{4+}$, with one of the 24-membered crown ether wheels, 24-crown-8 (**24C8**), dibenzo-24-crown-8 (**DB24C8**) or dinaphtho-24-crown-8 (**DN24C8**), in CD_3CN results in a ^{1}H NMR spectrum indicative of [2]pseudorotaxane formation; only $\mathbf{8}^{2+}$ containing the bulky *t*Bu substituent did not form an adduct.[16] These results can be divided into two groups in which: (1) the equilibrium between the free components and the pseudorotaxane is undergoing slow exchange on the NMR time scale and three different sets of peaks are observed, two corresponding to the free axle and the crown ether and the other to a new species, the [2]pseudorotaxane; and (2) the equilibrium is undergoing fast exchange on the NMR time scale and only a single, averaged set of resonances could be observed that were shifted from their original positions. Although there is no fundamental difference between these two sets of compounds other than the rates of threading and dethreading, for ease of discussion and since the slow exchange spectra provide more structural details the two cases will be discussed separately.

[2]Pseudorotaxanes at slow exchange

At slow exchange, the ^{1}H NMR chemical shifts of the new [2]pseudorotaxane species are clearly identifiable. The position of these resonances relative to their uncomplexed counterparts allows identification of the non-covalent interactions occurring between the two components and suggests that threading of the 1,2-bis(pyridinium)ethane axle through a '**24C8**' wheel gives rise to a [2]pseudorotaxane geometry. The resonance of the central ethane protons shift downfield which is characteristic of protons involved in hydrogen-bonding interactions, C–H · · · O. The hydrogen atoms in the *ortho*-N^+ position are also shifted downfield providing evidence of their participation in hydrogen bonding. In the case of the [2]pseudorotaxanes involving **DB24C8** and **DN24C8**, the *meta*-N^+ protons shift upfield because of the shielding generated by the ring current of the catechol units and indicates the presence of aromatic π-stacking interactions. As an example, Fig. 1 shows the changes in chemical shifts for $\mathbf{3a}^{2+}$ and **DB24C8** upon formation of the [2]pseudorotaxane $[\mathbf{3a}\subset\mathbf{DB24C8}]^{2+}$. It is clear that significant chemical shift changes occur for the participating protons of **3a** and **DB24C8** in the order of *ca.* 0.3–0.4 ppm. These chemical shift changes are summarized in Table 1 for [2]pseudorotaxanes formed from combining axles $\mathbf{1}^{2+}$, $\mathbf{2a}^{2+}$, $\mathbf{2b}^{2+}$, $\mathbf{3a}^{2+}$, $\mathbf{3b}^{2+}$ and $\mathbf{9}^{4+}$ with macrocycles **24C8**, **DB24C8** and **DN24C8**.

The chemical exchange process relating the uncomplexed and complexed species was confirmed by NMR Exchange Spectroscopy (EXSY).[17] The EXSY spectrum of $[\mathbf{3a}\subset\mathbf{DB24C8}]^{2+}$ is shown in Fig. 2, highlighting both exchanging resonances and peaks related by a NOE. Similar spectra were obtained for all combinations undergoing slow exchange and allowed unambiguous assignment for all resonances.

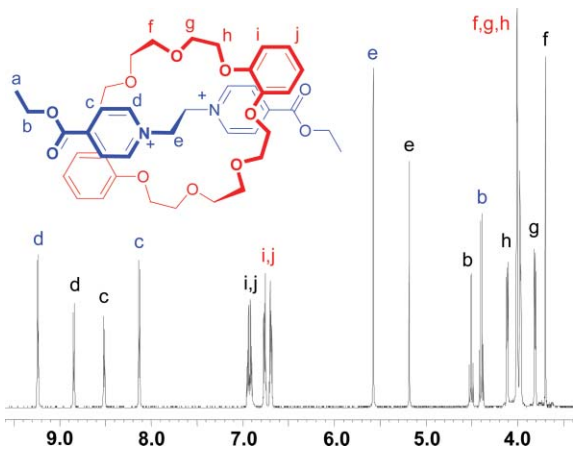

Fig. 1 ^{1}H NMR spectrum in CD_3CN at 2.0×10^{-3} M of an equimolar solution of $[\mathbf{3a}][BF_4]_2$ and **DB24C8** showing formation of $[\mathbf{3a}\subset\mathbf{DB24C8}]^{2+}$ (red and blue labels = complexed components of the [2]pseudorotaxane $[\mathbf{3a}\subset\mathbf{DB24C8}]^{2+}$, black labels = uncomplexed axle $\mathbf{3a}^{2+}$ and wheel **DB24C8**).

Table 1 ^{1}H NMR chemical shifts for axles and [2]pseudorotaxanes undergoing slow exchange on the NMR time scale

	CH_2N^+	H-*ortho*-N^+	H-*meta*-N^+
Compound	δ ($\Delta\delta$)	δ ($\Delta\delta$)	δ ($\Delta\delta$)
$[\mathbf{1}]^{2+}$	5.16	8.89	8.40
$[\mathbf{1}\subset\mathbf{24C8}]^{2+}$	5.36 (+0.20)	9.18 (+0.29)	8.44 (+0.04)
$[\mathbf{1}\subset\mathbf{DB24C8}]^{2+}$	5.56 (+0.40)	9.19 (+0.30)	8.04 (−0.36)
$[\mathbf{1}\subset\mathbf{DN24C8}]^{2+}$	5.61 (+0.45)	9.20 (+0.31)	7.97 (−0.43)
$[\mathbf{2a}]^{2+}$	5.13	8.68	8.34
$[\mathbf{2a}\subset\mathbf{24C8}]^{2+}$	5.34 (+0.21)	9.08 (+0.40)	8.39 (+0.05)
$[\mathbf{2a}\subset\mathbf{DB24C8}]^{2+}$	5.51 (+0.38)	9.06 (+0.38)	7.96 (−0.38)
$[\mathbf{2a}\subset\mathbf{DN24C8}]^{2+}$	5.54 (+0.41)	9.09 (+0.41)	7.86 (−0.48)
$[\mathbf{2b}]^{2+}$	5.22	9.06, 8.84	8.16
$[\mathbf{2b}\subset\mathbf{24C8}]^{2+}$	5.41 (+0.19)	9.44 (+0.38) 9.04 (+0.20)	8.21 (+0.05)
$[\mathbf{2b}\subset\mathbf{DB24C8}]^{2+}$	5.62 (+0.40)	9.43 (+0.37) 9.02 (+0.18)	7.75 (−0.41)
$[\mathbf{2b}\subset\mathbf{DN24C8}]^{2+}$	5.66 (+0.44)	9.46 (+0.40) 9.09 (+0.25)	7.77 (−0.39)
$[\mathbf{3a}]^{2+}$	5.24	8.96	8.52
$[\mathbf{3a}\subset\mathbf{24C8}]^{2+}$	5.40 (+0.16)	9.27 (+0.31)	8.56 (+0.04)
$[\mathbf{3a}\subset\mathbf{DB24C8}]^{2+}$	5.58 (+0.34)	9.25 (+0.29)	8.14 (−0.38)
$[\mathbf{3a}\subset\mathbf{DN24C8}]^{2+}$	5.61 (+0.37)	9.28 (+0.32)	8.07 (−0.45)
$[\mathbf{3b}]^{2+}$	5.22	9.39, 8.95	8.26
$[\mathbf{3b}\subset\mathbf{24C8}]^{2+}$	5.40 (+0.18)	9.71 (+0.32) 9.28 (+0.33)	8.27 (+0.01)
$[\mathbf{3b}\subset\mathbf{DB24C8}]^{2+}$	5.63 (+0.41)	9.71 (+0.32) 9.29 (+0.34)	7.92 (−0.34)
$[\mathbf{3b}\subset\mathbf{DN24C8}]^{2+}$	5.66 (+0.44)	9.72 (+0.33) 9.33 (+0.38)	7.92 (−0.34)
$[\mathbf{9}]^{4+}$	5.28	9.01	8.48
$[\mathbf{9}\subset\mathbf{24C8}]^{4+}$	5.44 (+0.16)	9.32 (+0.31)	8.54 (+0.06)
$[\mathbf{9}\subset\mathbf{DB24C8}]^{4+}$	5.62 (+0.34)	9.32 (+0.31)	8.16 (−0.32)
$[\mathbf{9}\subset\mathbf{DN24C8}]^{4+}$	5.67 (+0.39)	9.33 (+0.32)	8.17 (−0.31)

[2]Pseudorotaxanes at fast exchange

The 1,2-bis(pyridinium)ethane axles $\mathbf{4}^{2+}$, $\mathbf{5a}^{2+}$, $\mathbf{5b}^{2+}$, $\mathbf{6a}^{2+}$, $\mathbf{6b}^{2+}$, $\mathbf{7a}^{2+}$ and $\mathbf{7b}^{2+}$ also form [2]pseudorotaxanes with crown ethers **24C8**, **DB24C8** and **DN24C8**, but for these cases the chemical

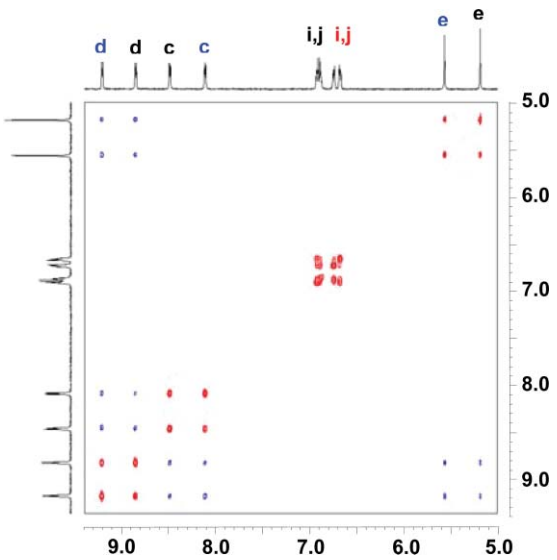

Fig. 2 Downfield portion of the EXSY spectrum of [**3a**⊂**DB24C8**]$^{2+}$ showing exchanging peaks (red) and peaks related by a NOE (blue). Labeling scheme is the same as Fig. 1.

exchange is fast on the NMR time scale, probably due to the smaller size of the substituents on the pyridinium ring which gives rise to a more rapid threading–unthreading rate.[18] This phenomenon allows the observation of only one set of averaged peaks in the ^{1}H NMR spectra; however, the limiting chemical shifts of the [2]pseudorotaxane species could be obtained from titration experiments employed to measure association constants, K_a (see ESI†). In the titration method, each axle was titrated with increasing amounts of crown ether until saturation was indicated. Table 2 lists chemical shifts for the [2]pseudorotaxanes undergoing fast exchange. The relative shifts of protons involved in hydrogen bonding and π-stacking is comparable to those observed for the [2]pseudorotaxanes under slow exchange. This suggests that the interpenetrated structure of the [2]pseudorotaxane is maintained regardless of the rate of the threading process from which it is formed.

Mass spectral evidence of [2]pseudorotaxane formation

[2]Pseudorotaxane formation was also detected using electrospray ionization mass spectrometry (ESI-MS). This is an ideal technique for observing charged organic compounds[19] and it is significant that this type of non-covalent interaction can be verified in such a facile manner at relatively low concentrations. In all cases, both the singly- and doubly-charged species [M − BF_4]$^+$ and [M]$^{2+}$ were observed with the expected isotopic profile and sufficient resolution for exact mass measurements. Fig. 3 shows the ESI mass spectrum of an equimolar solution of [**3a**][BF_4]$_2$ and **DB24C8** in MeCN at 1.0 × 10^{-6} M. Peaks for both the singly- and doubly-charged [2]pseudorotaxanes [**3a**⊂**DB24C8**·BF_4]$^+$ and [**3a**⊂**DB24C8**]$^{2+}$, as well as those for the axle [**3a**·BF_4]$^+$ and crown ether complex [Na⊂**DB24C8**]$^+$, were the only observed peaks.

Thermodynamic parameters for [2]pseudorotaxanes

When the rate of association and dissociation was slow on the NMR time scale, as indicated by the observation of both

Table 2 ^{1}H NMR chemical shifts for axles and [2]pseudorotaxanes undergoing fast exchange on the NMR time scale

	CH_2N^+	H-*ortho*-N^+	H-*meta*-N^+
Compound	δ ($\Delta\delta$)	δ ($\Delta\delta$)	δ ($\Delta\delta$)
[**4**]$^{2+}$	5.09	8.68	8.11
[**4**⊂**24C8**]$^{2+}$	5.33 (+0.24)	9.11 (+0.43)	8.14 (+0.03)
[**4**⊂**DB24C8**]$^{2+}$	5.43 (+0.34)	9.01 (+0.33)	7.69 (−0.42)
[**4**⊂**DN24C8**]$^{2+}$	5.44 (+0.35)	9.19 (+0.51)	7.70 (−0.41)
[**5a**]$^{2+}$	4.99	8.46	7.87
[**5a**⊂**24C8**]$^{2+}$	5.25 (+0.26)	8.93 (+0.47)	7.90 (+0.03)
[**5a**⊂**DB24C8**]$^{2+}$	5.33 (+0.34)	8.80 (+0.34)	7.43 (−0.44)
[**5a**⊂**DN24C8**]$^{2+}$	5.34 (+0.35)	8.87 (+0.41)	7.40 (−0.47)
[**5b**]$^{2+}$	5.02	8.52, 8.40	7.95
[**5b**⊂**24C8**]$^{2+}$	5.27 (+0.25)	9.03 (+0.51) 8.91 (+0.51)	8.01 (+0.06)
[**5b**⊂**DB24C8**]$^{2+}$	5.37 (+0.35)	8.83 (+0.31) 8.78 (+0.38)	7.56 (−0.39)
[**5b**⊂**DN24C8**]$^{2+}$	5.34 (+0.32)	8.90 (+0.38) 8.86 (+0.46)	7.49 (−0.46)
[**6a**]$^{2+}$	4.83	8.32	7.42
[**6a**⊂**24C8**]$^{2+}$	5.16 (+0.33)	8.87 (+0.55)	7.49 (+0.07)
[**6a**⊂**DB24C8**]$^{2+}$	5.21 (+0.38)	8.63 (+0.31)	6.98 (−0.44)
[**6a**⊂**DN24C8**]$^{2+}$	5.20 (+0.37)	8.82 (+0.50)	6.99 (−0.43)
[**6b**]$^{2+}$	5.04	8.40, 8.19	7.96
[**6b**⊂**24C8**]$^{2+}$	5.31 (+0.27)	8.93 (+0.53) 8.71 (+0.52)	8.02 (+0.06)
[**6b**⊂**DB24C8**]$^{2+}$	5.43 (+0.39)	8.79 (+0.39) 8.56 (+0.37)	7.55 (−0.41)
[**6b**⊂**DN24C8**]$^{2+}$	5.47 (+0.43)	8.92 (+0.52) 8.68 (+0.49)	7.51 (−0.45)
[**7a**]$^{2+}$	4.47	7.72	6.84
[**7a**⊂**24C8**]$^{2+}$	[a]	[a]	[a]
[**7a**⊂**DB24C8**]$^{2+}$	[b]	[b]	[b]
[**7a**⊂**DN24C8**]$^{2+}$	[b]	[b]	[b]
[**7b**]$^{2+}$	4.81	7.75, 7.64	7.59
[**7b**⊂**24C8**]$^{2+}$	5.14 (+0.33)	8.32 (+0.57) 8.18 (+0.54)	7.64 (+0.05)
[**7b**⊂**DB24C8**]$^{2+}$	5.15 (+0.34)	8.27 (+0.52) 7.98 (+0.34)	7.14 (−0.45)
[**7b**⊂**DN24C8**]$^{2+}$	5.08 (+0.27)	8.10 (+0.35) 7.99 (+0.35)	7.01 (−0.58)

[a] No discernable shifts were observed in the NMR spectra; no evidence of pseudorotaxane was found in the ESI-MS. [b] Very small shifts indicated probable pseudorotaxane formation but this is at the limit of detection. Pseudorotaxane formation was, however, observed in the ESI-MS.

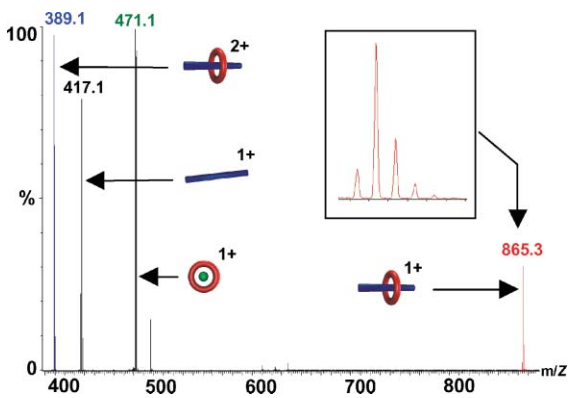

Fig. 3 ESI mass spectrum of an equimolar solution of [**3a**][BF_4]$_2$ and **DB24C8** in MeCN at 1.0 × 10^{-6} M. Peaks for naked axle [**3a**·BF_4]$^+$ (black), crown ether [Na⊂**DB24C8**]$^+$ (green) and both the singly- and doubly-charged [2]pseudorotaxanes [**3a**⊂**DB24C8**·BF_4]$^+$ (red) and [**3a**⊂**DB24C8**]$^{2+}$ (blue) are clearly visible.

Table 3 Complete listing of $K_a \times 10^2$ (M^{-1})[a] and $\Delta G°$ (kJ mol^{-1}) values for [2]pseudorotaxanes in CD_3CN solution (2×10^{-3} M) at 25 °C

	Crown ether wheel		
Axle	**24C8**	**DB24C8**	**DN24C8**
$[\mathbf{1}]^{2+}$	3.0 (−14.1)	9.3 (−16.9)	7.1 (−16.3)
$[\mathbf{2a}]^{2+}$	1.1 (−11.6)	4.0 (−14.8)	3.1 (−14.2)
$[\mathbf{2b}]^{2+}$	3.1 (−14.2)	3.5 (−14.5)	1.6 (−12.6)
$[\mathbf{3a}]^{2+}$	4.9 (−15.3)	19.4 (−18.8)	7.3 (−16.3)
$[\mathbf{3b}]^{2+}$	13.3 (−17.8)	47.4 (−21.0)	9.2 (−16.9)
$[\mathbf{4}]^{2+}$	1.9 (−13.0)	2.3 (−13.5)	0.9 (−11.0)
$[\mathbf{5a}]^{2+}$	1.1 (−11.7)	3.4 (−14.4)	1.6 (−12.6)
$[\mathbf{5b}]^{2+}$	1.7 (−12.8)	2.5 (−13.7)	1.8 (−12.8)
$[\mathbf{6a}]^{2+}$	0.6 (−10.1)	2.4 (−13.5)	0.7 (−10.5)
$[\mathbf{6b}]^{2+}$	1.5 (−12.4)	2.5 (−13.7)	1.7 (−12.7)
$[\mathbf{7a}]^{2+}$	*ca.* 0 (0.0)[b]	<0.1 (*ca.* −5)[c]	<0.1 (*ca.* −5)[c]
$[\mathbf{7b}]^{2+}$	0.5 (−9.5)	0.3 (−8.3)	0.3 (−8.3)
$[\mathbf{8}]^{2+}$	0.0 (0.0)[d]	0.0 (0.0)[d]	0.0 (0.0)[d]
$[\mathbf{9}]^{4+}$	2.0 (−13.2)	10.0 (−17.1)	13.3 (−17.8)

[a] Errors are estimated to be approximately 10% for association constants calculated from non-linear least-squares fit and less for those derived by the single point method. [b] No discernable shifts were observed in the NMR spectra; no evidence of pseudorotaxane was found in the ESI-MS. [c] Very small shifts indicated probable pseudorotaxane formation but this is at the limit of detection. Pseudorotaxane formation was, however, observed in the ESI-MS. [d] No changes were observed. This group is too large to allow threading.

complexed and uncomplexed species simultaneously in the ^{1}H NMR spectrum, the association constants (K_a) were measured by the single point method.[20] In the cases where only averaged signals were observed due to fast exchange, association constants were obtained from NMR titrations and a non-linear least-squares fit of the resulting saturation curves.[21] A complete listing of association constants (K_a) and related $\Delta G°$ values for [2]pseudorotaxane formation in CD_3CN solution (2×10^{-3} M) at 25 °C are compiled in Table 3.

The association constants vary from a low of *ca.* 0 M^{-1} for $[\mathbf{7a}\subset\mathbf{24C8}]^{2+}$ to a high of 47.4×10^2 M^{-1} for $[\mathbf{3b}\subset\mathbf{DB24C8}]^{2+}$. The variations are most easily visualized from Fig. 4 and Fig. 5 which display K_a as a function of crown ether for 4-substituted and 3-substituted axles respectively. Comparing axles we can make three general observations: (i) the maximum on both graphs occurs when the substituent on the axle is COOEt, (ii) the minimum on

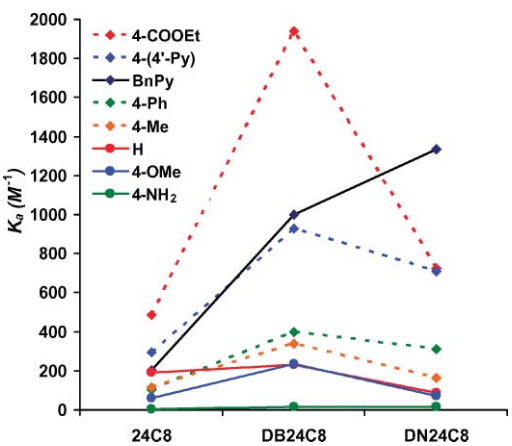

Fig. 4 Graph of K_a (at 25 °C) *versus* type of crown ether for [2]pseudorotaxanes with 4-substituted axles.

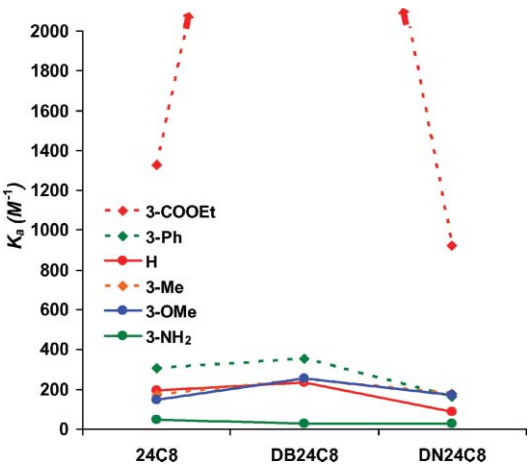

Fig. 5 Graph of K_a (at 25 °C) *versus* type of crown ether for [2]pseudorotaxanes with 3-substituted axles. The point representing $[\mathbf{3b}\subset\mathbf{DB24C8}]^{2+}$ has a K_a value of 47.4×10^2 M^{-1} and is omitted from the graph to allow visualization of the other values and direct comparison to Fig. 4.

both graphs occurs when the substituent is NH_2, and (iii) the effect of substitution on the pyridinium ring is more pronounced for the 3-substituted axles. These trends can be rationalized by noting that stronger electron withdrawing groups (such as COOEt) will produce more acidic axle hydrogen atoms as well as a greater positive charge at the pyridinium nitrogen, and substitution at the 3-position has a greater effect on the α-pyridinium protons which are involved in hydrogen bonding. A further reduction in K_a also occurs when the axle is $\mathbf{7a}^{2+}$ (X = NH_2, Y = H) due to significant contributions from a quinoid-like resonance structure which effectively removes the charge at the pyridinium N atom and places it on the amino group.[22]

Clearly, larger association constants are due to stronger hydrogen bonding and greater ion-dipole interactions. This trend is similar to that observed by Stoddart and co-workers for secondary dibenzylammonium axles in which the major interactions are the NH···O hydrogen bond and the N^+···O ion-dipole interaction.[23] Consistent with this explanation, Stoddart's group also reported that for secondary dibenzylammonium axles and 24-membered crown ethers, the binding strengths for a particular axle varied with crown ether such that **24C8** > **B24C8** > **DB24C8**.[24] Thus hydrogen bonding and ion-dipole interactions were greater for wheels containing aliphatic ether oxygen atoms rather than aromatic ether oxygen atoms. In contrast for this new templating motif, the maximum for each axle occurs for **DB24C8** (except $\mathbf{9}^{4+}$, X = Bnpy). This suggests that the increase in interaction energy as a result of the addition of π-stacking between the electron-poor pyridinium rings and electron-rich catechol rings surpasses or at least offsets the decrease in CH···O hydrogen bonding and the N^+···O ion-dipole interactions which must result from replacing four aliphatic ether oxygen atoms with less basic aromatic versions.

Interestingly, the only case for which a higher association constant occurs using the **DN24C8** wheel is when the two terminal nitrogen atoms of the thread $\mathbf{1}^{2+}$ are benzylated, giving rise to a tetracationic axle $\mathbf{9}^{4+}$. The increase in the magnitude of the K_a can be explained by a new interaction between the outer N^+ and the π-electron density of the naphthyl rings. In addition, there is also the possibility of a T-type, C–H···π interaction between aromatic

protons on the naphthyl ring and the face of the benzyl aromatic group.

A plot of $\log[K_a(X)/K_a(H)]$ *versus* the Hammett parameter,[25] σ, for the [2]pseudorotaxanes formed with **24C8** is almost linear (see Fig. 6) while the same plots for **DB24C8** and **DN24C8** are widely scattered (see also ESI†). This supports the notion that when significant π-stacking contributions are *not* present, the major interactions between wheel and axle are C–H · · · O hydrogen bonding and the N^+ · · · O ion-dipole which are directly affected by and can be controlled by the electronic nature of the substituents on the pyridinium rings.

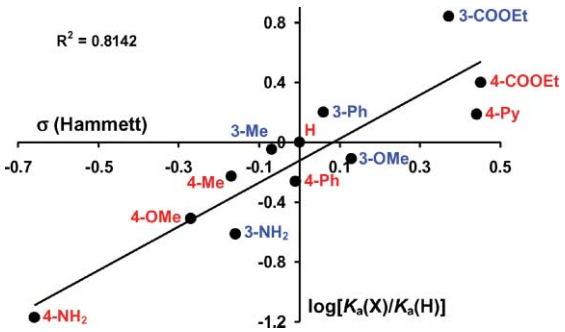

Fig. 6 Graph showing the correlation of $\log[K_a(X)/K_a(H)]$ with the Hammett constant (σ) for [2]pseudorotaxanes comprised of **24C8** and either 3-substituted (blue) or 4-substituted (red) axles.

^{1}H NMR studies at various temperatures were used to determinate the thermodynamic variables $\Delta H°$ and $\Delta S°$ for those adducts which were undergoing slow exchange on the NMR time scale; these are summarized in Table 4. Van't Hoff plots[26] in the temperature range of −30 to 30 °C were obtained for each [2]pseudorotaxane. Examples for axle **3a**$^{2+}$ with wheels **24C8**, **DB24C8** and **DN24C8** are shown in Fig. 7. The non-linearity of the plots for **24C8** and **DN24C8** is likely due to significant heat capacity contributions, and application of the Dougherty model[27] allowed monitoring of the variation of $\Delta G°$, $\Delta H°$ and $\Delta S°$ in the −30 to 30 °C temperature range. The ΔC_p values are all negative (from −293 to −1456 J mol^{-1} K^{-1}) which is representative of this type of inclusion process;[27] ΔC_p(**24C8**) < ΔC_p(**DN24C8**). It is clear that there is a dominance of the $\Delta H°$ term at high temperature and of the $T\Delta S°$ term at low temperature.

Table 4 Complete listing of $\Delta H°$ and $\Delta S°$ values for [2]pseudorotaxanes in CD_3CN solution at 25 °C

Compound	$\Delta H°$/kJ mol^{-1}	$\Delta S°$/J mol^{-1} K^{-1}
[1⊂24C8]$^{2+}$	−11.8	+7.4
[1⊂DB24C8]$^{2+}$	−60.8	−147.2
[1⊂DN24C8]$^{2+}$	−26.6	−34.7
[2a⊂24C8]$^{2+}$	−28.2	−55.8
[2a⊂DB24C8]$^{2+}$	−44.3	−98.8
[2a⊂DN24C8]$^{2+}$	−35.2	−70.5
[2b⊂24C8]$^{2+}$	−20.6	−21.5
[2b⊂DB24C8]$^{2+}$	−44.9	−101.8
[2b⊂DN24C8]$^{2+}$	−35.6	−77.0
[3a⊂24C8]$^{2+}$	−17.5	−7.3
[3a⊂DB24C8]$^{2+}$	−48.4	−99.4
[3a⊂DN24C8]$^{2+}$	−24.3	−26.7
[3b⊂24C8]$^{2+}$	−20.6	−9.2
[3b⊂DB24C8]$^{2+}$	−67.0	−154.5
[3b⊂DN24C8]$^{2+}$	−20.3	−11.5
[9⊂24C8]$^{4+}$	−20.0	−22.8
[9⊂DB24C8]$^{4+}$	−57.7	−136.2
[9⊂DN24C8]$^{4+}$	−12.4	+18.2

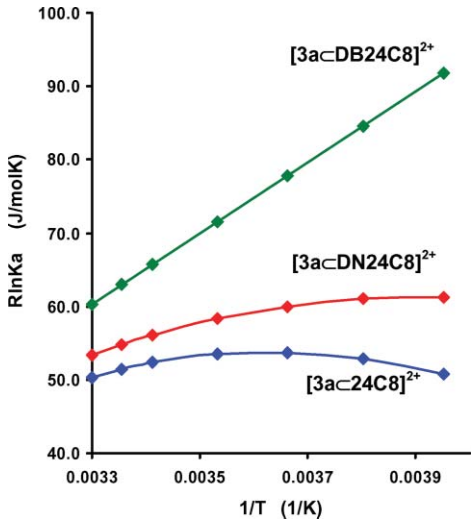

Fig. 7 Van't Hoff plots for the [2]pseudorotaxanes constructed from axle **3a**$^{2+}$ (4-COOEt) and wheels **DB24C8** (green), **DN24C8** (red) and **24C8** (blue).

In general, $\Delta H°$ values are significantly negative indicating strong interactions and a true molecular recognition process. An interesting observation is that for all axles, $\Delta H°$ is significantly more favorable and $\Delta S°$ significantly less favorable for complexation with **DB24C8**. Both these trends can be attributed to the efficient π-stacking contributions between these bis(pyridinium)ethane axles and this crown. This interaction is reflected in the enthalpic gain while the entropic loss is probably a result of limiting the rotational freedom of the aromatic rings of the axle.

The compensation in $\Delta H°$ and $\Delta S°$ to maintain an almost constant $\Delta G°$ over the range of temperature as seen in Fig. 8 for **[3a⊂24C8]**$^{2+}$ is characteristic of a number of larger supramolecular and biological systems.[28a] In this regard, an entropy–enthalpy compensation plot of $T\Delta S°$ *vs.* $\Delta H°$ for the [2]pseudorotaxanes listed in Table 4 shows a linear relationship with slope $\alpha = 0.94$

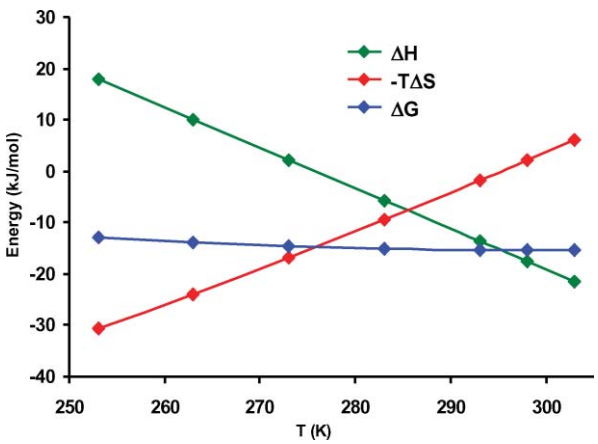

Fig. 8 Graph of the variation of $\Delta G°$, $\Delta H°$ and $-T\Delta S°$ from −30 to 30 °C for **[3a⊂24C8]**$^{2+}$ (X = COOEt, Y = H).

and a $T\Delta S°$ intercept = 13.9 kJ mol^{-1} (Fig. 9). Values of α between 0.8 and 1.2 are considered high and represent significant conformational changes, while $T\Delta S°$ values between 10 and 16 kJ mol^{-1} are attributed to important solvation effects occurring during complexation.[28] Both these observations are consistent with the formation of an interpentrated host–guest motif which must necessarily be accompanied by significant disruption to the solvation spheres and restrictions of the conformational flexibilty of the individual components.

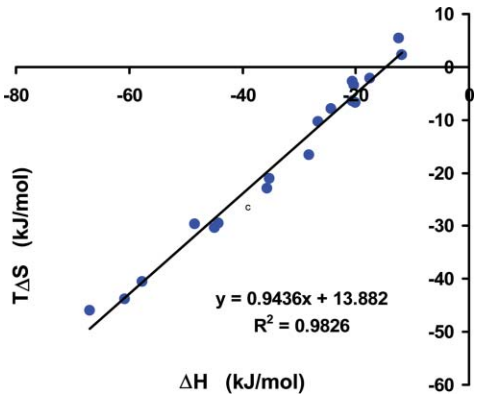

Fig. 9 Entropy–enthalpy compensation plot of $T\Delta S°$ *vs.* $\Delta H°$ for all the [2]pseudorotaxanes in Table 4 (slow exchange) shows a linear relationship with slope $\alpha = 0.94$ and a $T\Delta S°$ intercept = 13.9 kJ mol^{-1} (correlation, $R = 0.983$).

X-Ray structures

Although the solution NMR data for the adducts formed between a 1,2-bis(pyridinium)ethane cation and a 24-membered crown ether strongly indicate the formation of an interpenetrated complex, it was important to verify this by X-ray crystallography. The solid state structures also allow a detailed analysis of the non-covalent interactions contributing to the formation of the [2]pseudorotaxanes. We were able to obtain X-ray quality crystals for nine of these adducts and the results are presented in this section.

[2]Pseudorotaxanes with 24C8. The simplest example of a [2]pseudorotaxane in this series is [**4**⊂**24C8**]$^{2+}$, since there are no substituents on the pyridinium rings (X = H, Y = H) and no aromatic rings on the crown ether. Fig. 10[29] shows how the two components interpenetrate and details the various non-covalent interactions that occur. In particular, there is a significant interaction between the two positively charged pyridinium N atoms and two of the ether oxygen atoms (O3 and O7) at 3.24 and 3.28 Å. This is accompanied by eight C–H···O interactions from the four NCH_2 methylene hydrogen atoms and the four α-pyridinium hydrogen atoms to six of the oxygen atoms of the crown ether. The C···O distances range from 3.18 to 3.39 Å for the NCH_2 hydrogens and from 3.21 to 3.41 Å for the α-pyridinium hydrogens with the C–H···O angles from 140.1 to 151.9° for NCH_2 and from 135.6 to 160.4° for α-py. These are typical values for this type of weak hydrogen bond between a relatively acidic C–H bond and an electronegative O atom.[30] The relative orientation of axle and wheel results from the interplay of these non-covalent interactions. That is, the interaction between

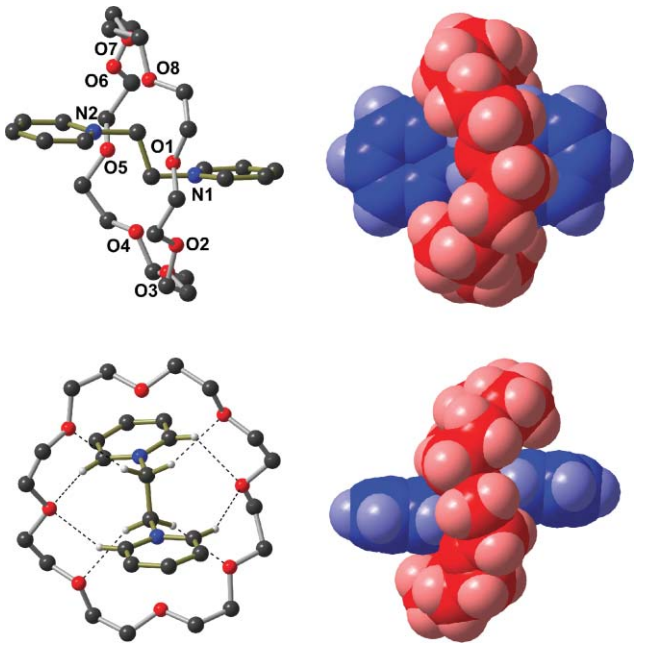

Fig. 10 X-Ray crystal structure of [**4**⊂**24C8**]$^{2+}$. Top-left: ball-and-stick representation with the numbering scheme (oxygen = red, nitrogen = blue, carbon = black, hydrogen = white). Bottom-left: view down the length of the molecule showing the eight C–H···O hydrogen bonds and the N$^+$···O interactions. Top-right: space-filling representation showing a top view (pyridinium axle = blue, crown ether wheel = red). Bottom-right: space-filling representation showing a side view.

the interior surface of the crown ether and the exterior surface of the 1,2-bis(pyridinium)ethane is optimized by the formation of the observed interpenetrated structure. Fig. 10 also shows space-filling models of [**4**⊂**24C8**]$^{2+}$ and emphasizes the snug fit between a 24-membered macrocycle and the pyridinium-based axle.

The structure of the adduct formed between **6b**$^{2+}$ containing a methoxy substituent in the 3-position of both pyridinium rings and **24C8** is shown in Fig. 11. Even though the presence of an electron donating group for [**6b**⊂**24C8**]$^{2+}$ lowers the association constant relative to [**4**⊂**24C8**]$^{2+}$ there is essentially no change in the interaction geometry. This is the first of many observations that lead to the conclusion that the effect of the substituents on the pyridinium rings is almost entirely electronic.

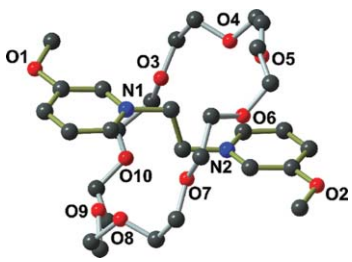

Fig. 11 X-Ray crystal structure of [**6b**⊂**24C8**]$^{2+}$ showing a ball-and-stick representation.

For the simple **24C8** macrocycle, there are no steric interactions between substituents at either the 3- or 4-positions of the pyridinium axle and the crown ether that would disrupt the non-covalent interactions on the interior of the [2]pseudorotaxane.

Although it is possible to affect the rate of threading by changing the axle substituents and to prevent threading completely by using a large *t*Bu group, these are not the result of steric interactions that alter the basic non-covalent interactions at the core of the [2]pseudorotaxane.

[2]Pseudorotaxanes with DB24C8. When **24C8** is replaced by **DB24C8**, there exists the possibility of π-stacking interactions between electron-poor pyridinium aromatic rings of the axle and electron-rich catechol rings on the crown ether.[31] In many ways, the archetypical structure of [2]pseudorotaxanes formed with this new motif is that formed between $\mathbf{1}^{2+}$ and commercially available **DB24C8**. Fig. 12 shows two ball-and-stick representations of the [2]pseudorotaxane [**1**⊂**DB24C8**]$^{2+}$ which emphasize the orientation of the linear pyridinium axle with respect to the cavity of the crown ether and the associated hydrogen bonding. The end-on view shows clearly how the eight hydrogen atoms of the axle (four NCH_2 methylene hydrogens and four aromatic, α-pyridinium hydrogens) align with the eight oxygen atoms of the crown ether and that the aromatic rings are parallel to optimize π-stacking. The overall interaction is very symmetrical with the axle and wheel essentially collinear; their long axes aligned parallel to each other. The methylene C···O distances range from 3.32 to 3.37 Å and the α-pyridinium C···O distances range from 3.27 to 3.32 Å. The centres of the crown ether aromatic rings are positioned directly over the bond linking the pyridinium and pyridine rings with a spacing of *ca.* 3.5 Å. This π-stacking is augmented by several $N^+ \cdots O$ ion-dipole interactions in the range 3.50–3.75 Å. Thus, unlike [**4**⊂**24C8**]$^{2+}$ for which two distinct $N^+ \cdots O$ ion-dipole interactions dictate the rotational orientation of axle and wheel, for [**1**⊂**DB24C8**]$^{2+}$ it is the π-stacking of the aromatic rings that controls this orientation. Fig. 12 also shows two space-filling representations of the structure which emphasize the π-stacking between the two components and demonstrate how the S-shaped conformation of **DB24C8** not only presents a large cavity which allows threading but also positions the electron-rich catechol rings over the electron-poor pyridinium rings of the axle.

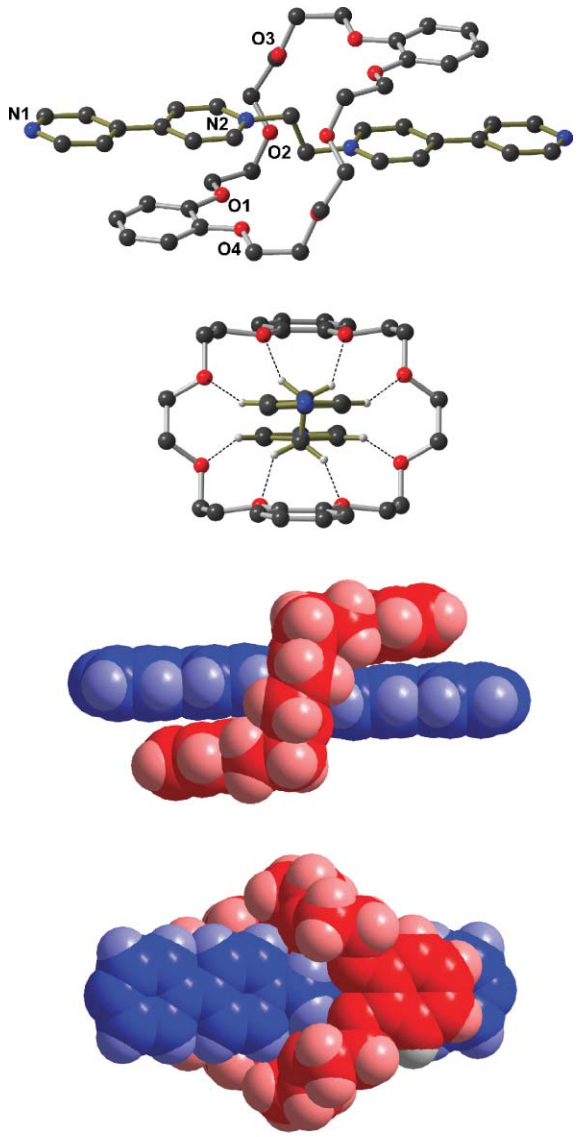

Fig. 12 X-Ray crystal structure of [**1**⊂**DB24C8**]$^{2+}$; the molecule has a crystallographically imposed centre of symmetry. Top: ball-and-stick representation. Second from top: view down the length of the molecule (end-on) showing the eight hydrogen bonds. Second from bottom: space-filling representation showing a side view of the π-stacking. Bottom: space-filling representation showing a top view of the π-stacking.

Replacing the 4-pyridyl unit on the axle with a phenyl group has a number of subtle effects on the overall structure as shown for [**2a**⊂**DB24C8**]$^{2+}$ in Fig. 13 (top). The major differences arise from the fact that changing from pyridyl to phenyl reduces the electron withdrawing effect on the pyridinium ring. The association constants are lower for all the [2]pseudorotaxanes with $\mathbf{2a}^{2+}$ relative to $\mathbf{1}^{2+}$ (see Table 3) due to reduced acidity of the axle hydrogens but this difference is largest for **DB24C8** when the effect of π-stacking is also reduced. In the structure [**2a**⊂**DB24C8**]$^{2+}$, the wheel and axle are not aligned in a collinear fashion as they are for [**1**⊂**DB24C8**]$^{2+}$ which would maximize π-stacking. Instead, there

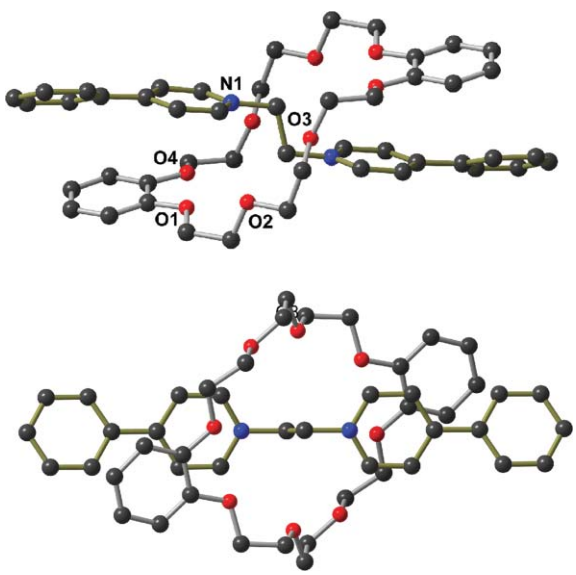

Fig. 13 X-Ray crystal structure of [**2a**⊂**DB24C8**]$^{2+}$; the molecule has a crystallographically imposed centre of symmetry. Top: a ball-and-stick representation. Bottom: the orientation of axle and wheel positions the catechol oxygen atoms over the pyridinium nitrogen atoms.

is a shift which positions one of the catechol oxygen atoms over the positively charged pyridinium atom (3.59 Å) reminiscent of what was observed for the **24C8** structures when there was no possibility of π-stacking, see Fig. 13 (bottom).

When the substituent on the axle is a good electron withdrawing group such as the ester function COOEt, the association constants for pseudorotaxane formation are the highest for all crown ethers. Interestingly, neither the structure of [**3a**⊂**DB24C8**]$^{2+}$ nor [**3b**⊂**DB24C8**]$^{2+}$, which are shown in Fig. 14, display any unique structural features which might account for this observation. Again, we conclude that the increase in stability for these particular [2]pseudorotaxanes is due almost entirely to the electronic effects of the withdrawing groups which control the acidity of the hydrogen atoms involved in hydrogen bonding and the relative charge density residing on the pyridinium nitrogen atoms. These effects reach a maximum for [**3b**⊂**DB24C8**]$^{2+}$ which has the COOEt function in the 3-position of the pyridinium ring.

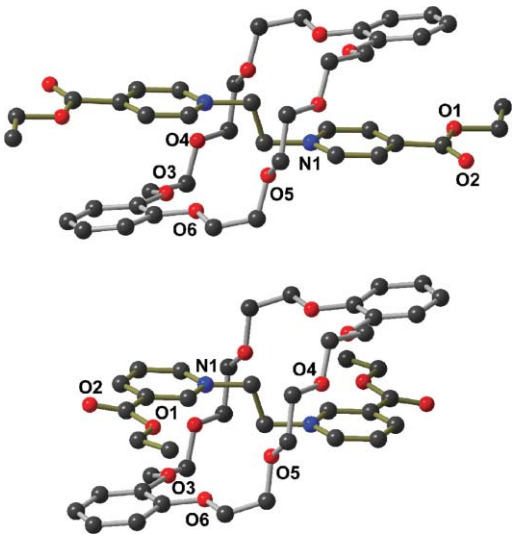

Fig. 14 X-Ray crystal structures of [**3a**⊂**DB24C8**]$^{2+}$ (top) and [**3b**⊂**DB24C8**]$^{2+}$ (bottom) showing a ball-and-stick representation; both molecules have crystallographically imposed centres of symmetry.

[2]Pseudorotaxanes with DN24C8. The major reason for investigating **DN24C8**[32] as the wheel in this templating motif was the potential of increasing the amount of π-stacking between axle and wheel, and thereby increasing the stability of the [2]pseudorotaxanes. However, as can be seen from the graphical and tabular data presented, in general the use of **DN24C8** did not result in an increase in the association constant (see again Table 3). The X-ray structures of [**1**⊂**DN24C8**]$^{2+}$ (top) and [**2a**⊂**DN24C8**]$^{2+}$ (bottom) are shown in Fig. 15. The structures are very similar to those observed for [**1**⊂**DB24C8**]$^{2+}$ [Fig. 12 (top)] and [**2a**⊂**DB24C8**]$^{2+}$ [Fig. 13 (top)]. It must be that the π-stacking interaction between the extended aromatic surface of the naphtho group and the 4-py or 4-Ph substituent is minimal. This could be due to the fact that neither of the terminal aromatic rings is particularly electron-poor relative to the pyridinium ring, and the naphtho aromatic ring is not as electron-rich as the catechol ring of **DB24C8**. Another consideration is that there may actually be a negative steric interaction between the substituent, which is free to rotate,

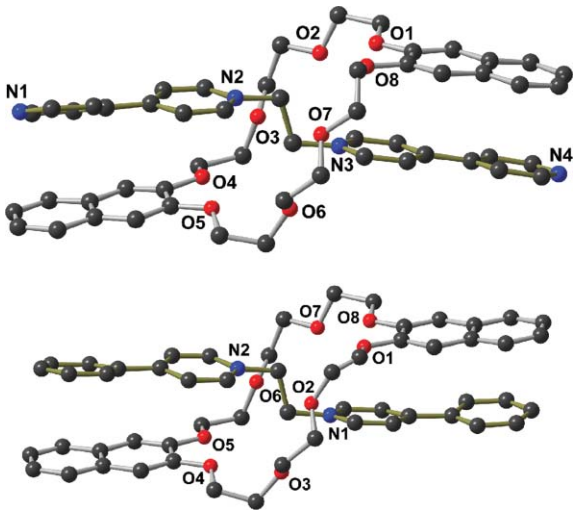

Fig. 15 X-Ray crystal structures of [**1**⊂**DN24C8**]$^{2+}$ (top) and [**2a**⊂**DN24C8**]$^{2+}$ (bottom) showing ball-and-stick representations.

and the extended aromatic ring of the crown ether. Although this can also occur for **DB24C8** this is presumably offset by larger π-stacking contributions.

The only example in which the use of **DN24C8** in place of **DB24C8** leads to an increase in association constant at 25 °C occurs for the axle terminated by a further pyridinium group: axle **9**$^{4+}$. The structure of the [2]pseudorotaxane [**9**⊂**DN24C8**]$^{4+}$ is shown in Fig. 16. The increase in association constant for this adduct relative to that with **DB24C8** and compared to others with **DN24C8** can be attributed to three features not present in the other pseudorotaxanes involving **DN24C8**. Firstly, the axle contains another electron-poor pyridinium ring which can undergo significant π-stacking interactions; second, the axle is now a tetracation which improves the electrostatic component of the interaction; and third, there appears to be a significant C–H · · · π interaction between one of the naphtho aromatic protons and the aromatic ring of the capping benzyl group; the C–H · · · centroid distance is 2.84 Å with a C–H–centroid angle of 149°.

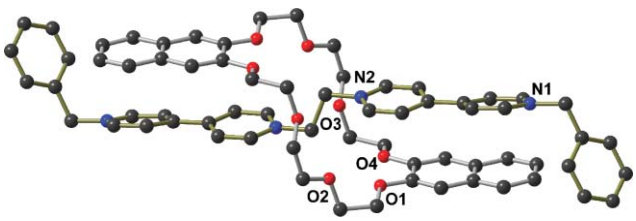

Fig. 16 X-Ray crystal structure of [**9**⊂**DN24C8**]$^{4+}$ showing a ball-and-stick representation; the molecule has a crystallographically imposed centre of symmetry.

Conclusions

We have shown that the combination of linear 1,2-bis-(pyridinium)ethane axles and 24-membered crown ether wheels (**24C8**, **DB24C8** and **DN24C8**) is a versatile templating motif for the formation of [2]pseudorotaxanes. Both solution and solid state evidence unambiguously demonstrate that these interpenetrated adducts are held together by N$^+$ · · · O ion-dipole interactions, a

series of C–H · · · O hydrogen bonds and when possible significant π-stacking interactions between electron-poor pyridinium rings of the axle and electron-rich catechol rings of the wheel. It was shown that the strength of the non-covalent interactions can be controlled by varying the nature of the substituent on the axle pyridinium rings with electron withdrawing groups providing increased hydrogen bonding and electrostatic interactions and therefore an increase in the stability of the system. Unlike simple alkylammonium axles which show higher association constants with **24C8** as compared to **DB24C8**, this motif demonstrates very significant contributions from π-stacking and exhibits higher association constants for **DB24C8**. In this regard, we have also shown that the use of a wheel with an extended π-system such as is the case for **DN24C8** can result in a further increase in stability for certain types of axles elaborated with further pyridinium groups.

The [2]pseudorotaxanes formed with axles $\mathbf{1}^{2+}$ or $\mathbf{9}^{4+}$ and the simple alkylation reaction required to convert axle $\mathbf{1}^{2+}$ to $\mathbf{9}^{4+}$ demonstrate a simple methodology for further functionalizing the axles without disrupting the basic templating interactions. Since no [2]pseudorotaxane was formed with axle $\mathbf{8}^{2+}$, together these readily provide a convenient route for the preparation of permanently interlocked [*n*]rotaxanes by utilizing *t*Bu-benzyl rather than benzyl as an alkylating group to yield the corresponding [2]rotaxane[9] (Fig. 17).

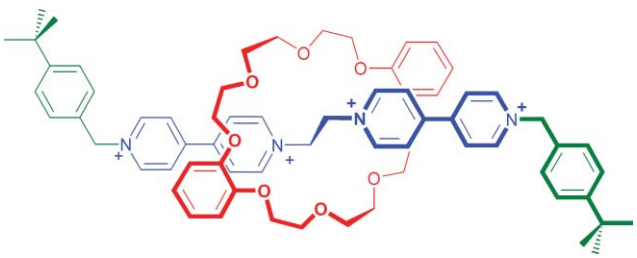

Fig. 17 [2]Rotaxane constructed using a 1,2-bis(4,4′-dipyridinium)ethane axle and **DB24C8** stoppered with bulky *t*Bu-benzyl groups.

Experimental

General

All chemicals were purchased from Aldrich Chemicals and used without further purification. The solvents were dried and distilled prior to use. ^{1}H NMR spectra were recorded on Brüker Avance 500 locked to the deuterated solvent operating at 500 MHz. Mass spectra were performed on a Micromass LCT electrospray ionization ToF spectrometer.

General procedure for the syntheses of the 1,2-bis(pyridinium)ethane tetrafluoroborate salts

1.000 g (5.3 mmol) of 1,2-dibromoethane and 5 equiv. of the corresponding pyridine were combined with 50 mL of acetonitrile and the solution refluxed between 24 and 72 h. The reaction mixture was cooled to room temperature, filtered and the solid washed with diethyl ether and dried under vacuum. The solid was combined with 10 mL of saturated aqueous NH_4BF_4 solution and brought to boiling until the solid was completely dissolved. The solution was immediately removed from the heat and allowed to cool slowly to room temperature to yield the 1,2-bis(pyridinium)ethane tetrafluoroborate salt as a white crystalline solid. All yields are reported as the bromide salts.

1,2-Bis(4,4′-dipyridyl)ethane[BF_4]$_2$, 1·(BF_4)$_2$. Yield = 74%. ^{1}H NMR (CD_3CN): δ (ppm) 8.89 (d, 4H, J = 5.9 Hz, *ortho*-N^+) 8.75 (d, 4H, J = 6.6 Hz, *ortho*-N), 8.40 (d, 4 H, *meta*-N^+), 7.83 (d, 4 H, *meta*-N), 5.16 (s, 4H, CH_2–N^+). HR-ESI-MS: m/z [**1**·BF_4]$^+$ calc.: 427.1717, found: 427.1716.

1,2-Bis(4-phenyl-1-pyridyl)ethane[BF_4]$_2$, 2a·(BF_4)$_2$. Yield = 41%. ^{1}H NMR (CD_3CN): δ (ppm) 8.68 (d, 4H, J = 6.8 Hz, *ortho*-N^+), 8.34 (d, 4H, *meta*-N^+), 7.97 (m, 4H, *ortho*-Ph), 7.70 (m, 6H, *meta*- and *para*-Ph), 5.13 (s, 4H, CH_2–N^+). HR-ESI-MS: m/z [**2a**·BF_4]$^+$ calc.: 425.1812, found: 425.1833.

1,2-Bis(3-phenyl-1-pyridyl)ethane[BF_4]$_2$, 2b·(BF_4)$_2$. Yield = 45%. ^{1}H NMR (CD_3CN): δ (ppm) 9.06 (s, 2H, *ortho*-N^+ and *ortho*-Ph), 8.84 (d, 2H, J = 7.1 Hz, *ortho*-N^+), 8.65 (d, 2H, J = 6.0 Hz, *para*-N^+), 8.16 (dd, 2H, *meta*-N^+), 7.77 (d, 4H, J = 6.9 Hz, *ortho*-Ph), 7.65 (m, 6H, *meta*- and *para*-Ph), 5.22 (s, 4H, CH_2–N^+). HR-ESI-MS: m/z [**2b**·BF_4]$^+$ calc.: 425.1812, found: 425.1805.

1,2-Bis(4-ethylester-1-pyridyl)ethane[BF_4]$_2$, 3a·(BF_4)$_2$. Yield = 7.4%. ^{1}H NMR (CD_3CN): δ (ppm) 8.96 (d, 4H, J = 6.7 Hz, *ortho*-N^+), 8.52 (d, 4H, *meta*-N^+), 5.24 (s, 4H, CH_2–N^+), 4.51 (q, 4H, J = 7.1 Hz, CH_2-α-COO), 1.44 (t, 6H, CH_3). HR-ESI-MS: m/z [**3a**·BF_4]$^+$ calc.: 417.1609, found: 417.1620.

1,2-Bis(3-ethylester-1-pyridyl)ethane[BF_4]$_2$, 3b·(BF_4)$_2$. Yield = 9.1%. ^{1}H NMR (CD_3CN): δ (ppm) 9.39 (s, 2H, *ortho*-N^+ and *ortho*-COOEt), 9.07 (d, 2H, J = 8.8 Hz, *para*-N^+), 8.95 (d, 2H, J = 6.2 Hz, *ortho*-N^+), 8.26 (dd, 2H, *meta*-N^+), 5.22 (s, 4H, CH_2–N^+), 4.51 (q, 4H, J = 7.1 Hz, CH_2-α-COO), 1.44 (t, 6H, CH_3). HR-ESI-MS: m/z [**3b**·BF_4]$^+$ calc.: 417.1609, found: 417.1624.

1,2-Bis(1-pyridyl)ethane[BF_4]$_2$, 4·(BF_4)$_2$. Yield = 21%. ^{1}H NMR (CD_3CN): δ (ppm) 8.68 (d, 4H, J = 5.5 Hz, *ortho*-N^+), 8.63 (t, 2H, J = 7.7 Hz, *para*-N^+), 8.11 (ps-t, 4H, *meta*-N^+), 5.09 (s, 4H, CH_2–N^+). HR-ESI-MS: m/z [**4**·BF_4]$^+$ calc.: 273.1186, found: 273.1185.

1,2-Bis(4-methyl-1-pyridyl)ethane[BF_4]$_2$, 5a·(BF_4)$_2$. Yield = 39%. ^{1}H NMR (CD_3CN): δ (ppm) 8.46 (d, 4H, J = 6.8 Hz, *ortho*-N^+), 7.87 (d, 4H, *meta*-N^+), 4.99 (s, 4H, CH_2–N^+), 2.67 (s, 6H, CH_3). HR-ESI-MS: m/z [**5a**·BF_4]$^+$ calc.: 301.1499, found: 301.1502.

1,2-Bis(3-methyl-1-pyridyl)ethane[BF_4]$_2$, 5b·(BF_4)$_2$. Yield = 40%. ^{1}H NMR (CD_3CN): δ (ppm) 8.52 (s, 2H, *ortho*-N^+ and *ortho*-CH_3), 8.40 (d, 2H, J = 8.1 Hz, *ortho*-N^+), 8.43 (d, 2H, J = 6.1 Hz, *para*-N^+), 7.95 (dd, 2H, *meta*-N^+), 5.02 (s, 4H, CH_2–N^+), 2.54 (s, 6H, CH_3). HR-ESI-MS: m/z [**5b**·BF_4]$^+$ calc.: 301.1499, found: 301.1494.

1,2-Bis(4-methoxy-1-pyridyl)ethane[BF_4]$_2$, 6a·(BF_4)$_2$. Yield = 42%. ^{1}H NMR (CD_3CN): δ (ppm) 8.32 (d, 4H, J = 7.6 Hz, *ortho*-N^+), 7.42 (d, 4H, *meta*-N^+), 4.83 (s, 4H, CH_2–N^+), 4.12 (s, 6H, OCH_3). HR-ESI-MS: m/z [**6a**·BF_4]$^+$ calc.: 333.1397, found: 333.1395.

1,2-Bis(3-methoxy-1-pyridyl)ethane[BF_4]$_2$, 6b·(BF_4)$_2$. Yield = 39%. ^{1}H NMR (CD_3CN): δ (ppm) 8.40 (s, 2H, *ortho*-N^+ and *ortho*-OCH_3), 8.19 (d, 2H, J = 5.8 Hz, *ortho*-N^+), 8.14 (dd, 2H,

$J_{m-p} = 8.7$, $J_{o-p} = 2.1$ Hz, *para*-N^+), 7.96 (dd, 2H, *meta*-N^+), 5.04 (s, 4H, CH_2–N^+), 4.03 (s, 6H, OCH_3). HR-ESI-MS: m/z [**6b**·BF_4]$^+$ calc.: 333.1397, found: 333.1409.

1,2-Bis(4-amino-1-pyridyl)ethane[BF_4]$_2$, 7a·(BF_4)$_2$. Yield = 42%. ^{1}H NMR (CD_3CN): δ (ppm) 7.72 (d, 4H, $J = 7.4$ Hz, *ortho*-N^+), 6.84 (d, 4H, *meta*-N^+), 6.74 (br, 4H, NH_2), 4.47 (s, 4H, CH_2–N^+). HR-ESI-MS: m/z [**7a**·BF_4]$^+$ calc.: 303.1404, found: 303.1419.

1,2-Bis(3-amino-1-pyridyl)ethane[BF_4]$_2$, 7b·(BF_4)$_2$. Yield = 40%. ^{1}H NMR (CD_3CN): δ (ppm) 7.75 (s, 2H, *ortho*-N^+ and *ortho*-NH_2), 7.64 (m, 4H, *ortho*-N^+ overlapped with *para*-N^+), 7.59 (m, 2H, *meta*-N^+), 5.49 (br, 4H, NH_2), 4.81 (s, 4H, CH_2–N^+). HR-ESI-MS: m/z [**7b**·BF_4]$^+$ calc.: 303.1404, found: 303.1394.

1,2-Bis(4-*t*-butyl-1-pyridyl)ethane[BF_4]$_2$, 8·(BF_4)$_2$. Yield = 47%. ^{1}H NMR (CD_3CN): δ (ppm) 8.61 (d, 4H, $J = 6.5$ Hz, *ortho*-N^+), 8.08 (d, 4H, *meta*-N^+), 5.04 (s, 4H, CH_2–N^+), 1.42 (s, 18H, CH_3). HR-ESI-MS: m/z [**8**·BF_4]$^+$ calc.: 385.2438, not found.

1,2-Bis(4′-benzyl-4,4′-dipyridyl)ethane[BF_4]$_4$, 9·(BF_4)$_4$. Compound **1**·[BF_4]$_2$ (165 mg, 0.33 mmol) was mixed with 4 equiv. of benzyl bromide in 40 mL of a 1 : 1 mixture of water–nitromethane containing an excess of Na[BF_4]. The mixture was stirred for two days and the product was isolated in 28% yield after removal of solvent and recrystallization from acetonitrile. ^{1}H NMR (CD_3CN): δ (ppm) 9.00 (d, 4H, $J = 6.3$ Hz, *ortho*-N^+–Bn) 8.98 (d, 4H, $J = 6.8$ Hz, *ortho*-N^+–Et), 8.48 (d, 4H, *meta*-N^+–Et), 8.43 (d, 4H, *meta*-N^+–Bn), 7.53 (m, 10H, *ortho*-, *meta*- and *para*-Ph), 5.85 (s, 4H, Bn), 5.27 (s, 4H, CH_2–N^+). HR-ESI-MS: m/z [**9**·(BF_4)$_3$]$^+$ calc.: 783.2871, found: 783.2832.

[1⊂24-Crown-8][BF_4]$_2$. ^{1}H NMR (CD_3CN): δ (ppm) 9.18 (broad, 4H, *ortho*-N^+), 8.90 (d, 4H, $J = 5.4$ Hz, *ortho*-N), 8.44 (d, 4H, $J = 6.1$ Hz, *meta*-N^+), 7.88 (d, 4H, *meta*-N), 5.36 (s, 4H, CH_2–N^+), 3.56 (s, 32H, CH_2-crown). HR-ESI-MS: m/z [**1**⊂**24C8**·BF_4]$^+$ calc.: 779.3814, found: 779.3821.

[1⊂Dibenzo-24-crown-8][BF_4]$_2$. ^{1}H NMR (CD_3CN): δ (ppm) 9.19 (broad, 4H, *ortho*-N^+), 8.82 (broad, 4H, *ortho*-N), 8.04 (broad, 4H, *meta*-N^+), 7.50 (broad, 4H, *meta*-N), 6.68 (m, 4H, *ortho*-O), 6.57 (m, 4H, *meta*-O), 5.56 (s, 4H, CH_2–N^+), 4.03 (m, 24H, α-, β- and γ-OCH_2). HR-ESI-MS: m/z [**1**⊂**DB24C8**·BF_4]$^+$ calc.: 875.3814, found: 875.3831.

[1⊂Dinaphtho-24-crown-8][BF_4]$_2$. ^{1}H NMR (CD_3CN): δ (ppm) 9.20 (broad, 4H, *ortho*-N^+), 8.43 (broad, 4H, *ortho*-N), 7.97 (broad, 4H, *meta*-N^+), 7.24 (broad, 4H, *meta*-N), 7.68 (broad, 4H, *ortho*-crown), 7.30 (broad, 4H, *meta*-crown), 6.94 (s, 4H, *ortho*-O-crown), 5.61 (s, 4H, CH_2–N^+), 4.32 (broad, 8H, α-OCH_2), 3.91 (broad, 8H, β-OCH_2), 3.78 (broad, 8H, γ-OCH_2). HR-ESI-MS: m/z [**1**⊂**DN24C8**·BF_4]$^+$ calc.: 975.4127, found: 975.4146.

[2a⊂24-Crown-8][BF_4]$_2$. ^{1}H NMR (CD_3CN): δ (ppm) 9.08 (d, 4H, $J = 6.7$ Hz, *ortho*-N^+), 8.39 (d, 4H, $J = 7.8$ Hz, *meta*-N^+), 8.01 (d, 4H, $J = 6.4$ Hz, *ortho*-Ph), 6.79 (m, 6H, *meta*- and *para*-Ph), 5.34 (s, 4H, CH_2–N^+), 3.53 (s, 32H, CH_2-crown). HR-ESI-MS: m/z [**2a**⊂**24C8**·BF_4]$^+$ calc.: 777.3909, found: 777.3920.

[2a⊂Dibenzo-24-crown-8][BF_4]$_2$. ^{1}H NMR (CD_3CN): δ (ppm) 9.06 (d, 4H, $J = 6.8$ Hz, *ortho*-N^+), 7.96 (d, 4H, *meta*-N^+), 7.67 (m, 10H, *ortho*-, *meta*- and *para*-Ph), 6.68 (m, 4H, *ortho*-O), 6.57 (m, 4H, *meta*-O), 5.51 (s, 4H, CH_2–N^+), 4.06 (m, 8H, α-OCH_2), 3.99 (m, 16H, β- and γ-OCH_2). HR-ESI-MS: m/z [**2a**⊂**DB24C8**·BF_4]$^+$ calc.: 873.3909, found: 873.3929.

[2a⊂Dinaphtho-24-crown-8][BF_4]$_2$. ^{1}H NMR (CD_3CN): δ (ppm) 9.09 (d, 4H, $J = 7.0$ Hz, *ortho*-N^+), 7.86 (d, 4H, *meta*-N^+), 7.69 (m, 4H, *meta*- and *para*-Ph), 7.07 (m, 4H, *ortho*-Ph), 7.45 (m, 4H, *ortho*-crown), 7.32 (m, 4H, *meta*-crown), 7.00 (s, 4H, *ortho*-O-crown), 5.54 (s, 4H, CH_2–N^+), 4.19 (m, 8H, α-OCH_2), 4.08 (m, 8H, β-OCH_2), 4.05 (s, 8H, γ-OCH_2). HR-ESI-MS: m/z [**2a**⊂**DN24C8**·BF_4]$^+$ calc.: 973.4222, found: 973.4226.

[2b⊂24-Crown-8][BF_4]$_2$. ^{1}H NMR (CD_3CN): δ (ppm) 9.44 (s, 2H, *ortho*-N^+ and *ortho*-Ph), 9.04 (d, 2H, $J = 6.0$ Hz, *ortho*-N^+), 8.81 (d, 2H, $J = 8.0$ Hz, *para*-N^+), 8.21 (dd, 2H, *meta*-N^+), 7.83 (m, 4H, *ortho*-Ph), 7.68 (m, 6H, *meta*- and *para*-Ph), 5.41 (s, 4H, CH_2–N^+), 3.45 (s, 32H, CH_2-crown). HR-ESI-MS: m/z [**2b**⊂**24C8**·BF_4]$^+$ calc.: 777.3909, found: 777.3927.

[2b⊂Dibenzo-24-crown-8][BF_4]$_2$. ^{1}H NMR (CD_3CN): δ (ppm) 9.43 (s, 2H, *ortho*-N^+ and *ortho*-Ph), 9.02 (d, 2H, $J = 5.5$ Hz, *ortho*-N^+), 8.29 (d, 2H, $J = 8.0$ Hz, *para*-N^+), 7.75 (dd, 2H, *meta*-N^+), 7.65 (m, 6H, *meta*- and *para*-Ph), 7.59 (m, 4H, *ortho*-Ph), 6.80 (m, 4H, *ortho*-O), 6.63 (m, 4H, *meta*-O), 5.62 (s, 4H, CH_2–N^+), 3.97 (m, 8H, α-OCH_2), 3.91 (m, 8H, β-OCH_2), 3.86 (s, 8H, γ-OCH_2). HR-ESI-MS: m/z [**2b**⊂**DB24C8**·BF_4]$^+$ calc.: 873.3909, found: 873.3882.

[2b⊂Dinaphtho-24-crown-8][BF_4]$_2$. ^{1}H NMR (CD_3CN): δ (ppm) 9.46 (s, 2H, *ortho*-N^+ and *ortho*-Ph), 9.09 (d, 2H, $J = 6.5$ Hz, *ortho*-N^+), 8.11 (d, 2H, $J = 8.5$ Hz, *para*-N^+), 7.77 (m, 2H, *meta*-N^+), 7.56 (d, 4H, $J = 7.5$ Hz, *ortho*-Ph), 7.50 (m, 6H, *meta*- and *para*-Ph), 7.61 (m, 4H, *ortho*-crown), 7.37 (m, 4H, *meta*-crown), 6.94 (s, 4H, *ortho*-O-crown), 5.66 (s, 4H, CH_2–N^+), 4.10 (m, 8H, α-OCH_2), 3.99 (m, 8H, β-OCH_2), 3.94 (s, 8H, γ-OCH_2). HR-ESI-MS: m/z [**2b**⊂**DN24C8**·BF_4]$^+$ calc.: 973.4222, found: 973.4223.

[3a⊂24-Crown-8][BF_4]$_2$. ^{1}H NMR (CD_3CN): δ (ppm) 9.27 (d, 4H, $J = 6.8$ Hz, *ortho*-N^+), 8.56 (d, 4H, $J = 7.8$ Hz, *meta*-N^+), 5.40 (s, 4H, CH_2–N^+), 4.51 (q, 4H, $J = 7.1$ Hz, CH_2-α-COO), 3.50 (s, 32H, CH_2-crown), 1.44 (t, 6H, CH_3). HR-ESI-MS: m/z [**3a**⊂**24C8**·BF_4]$^+$ calc.: 769.3706, found: 769.3730.

[3a⊂Dibenzo-24-crown-8][BF_4]$_2$. ^{1}H NMR (CD_3CN): δ (ppm) 9.25 (d, 4H, $J = 6.6$ Hz, *ortho*-N^+), 8.14 (d, 4H, $J = 7.8$ Hz, *meta*-N^+), 6.76 (m, 4H, *ortho*-O), 6.70 (m, 4H, *meta*-O), 5.58 (s, 4H, CH_2–N^+), 4.40 (q, 4H, $J = 7.13$ Hz, CH_2-α-COO), 4.00 (m, 24H, α-, β- and γ-OCH_2), 1.43 (t, 6H, CH_3). HR-ESI-MS: m/z [**3a**⊂**DB24C8**·BF_4]$^+$ calc.: 865.3706, found: 865.3738.

[3a⊂Dinaphtho-24-crown-8][BF_4]$_2$. ^{1}H NMR (CD_3CN): δ (ppm) 9.28 (d, 4H, $J = 6.6$ Hz, *ortho*-N^+), 8.07 (d, 4H, *meta*-N^+), 7.63 (m, 4H, *ortho*-Np), 7.34 (m, 4H, *meta*-Np), 7.03 (s, 4H, *ortho*-O), 5.61 (s, 4H, CH_2–N^+), 4.14 (m, 8H, α-OCH_2), 4.05 (m, 16H, β- and γ-OCH_2), 3.82 (q, 4H, $J = 7.13$ Hz, CH_2-α-COO), 1.12 (t, 6H, CH_3). HR-ESI-MS: m/z [**3a**⊂**DN24C8**·BF_4]$^+$ calc.: 965.4019, found: 965.4047.

[3b⊂24-Crown-8][BF_4]$_2$. ^{1}H NMR (CD_3CN): δ (ppm) 9.71 (s, 2H, *ortho*-N^+ and *ortho*-COOEt), 9.28 (d, 2H, $J = 5.2$ Hz, *ortho*-N^+), 9.06 (d, 2H, $J = 7.8$ Hz, *para*-N^+), 8.27 (dd, 2H, *meta*-N^+), 5.40 (s, 4H, CH_2–N^+), 4.54 (broad m, 4H, CH_2-α-COO), 3.51 (s, 32H, CH_2-crown), 1.45 (broad m, 6H, CH_3). HR-ESI-MS: m/z [**3b**⊂**24C8**·BF_4]$^+$ calc.: 769.3706, found: 769.3733.

[3b⊂Dibenzo-24-crown-8][BF_4]$_2$. ^{1}H NMR (CD_3CN): δ (ppm) 9.71 (s, 2H, *ortho*-N^+ and *ortho*-COOEt), 9.29 (d, 2H, $J = 6.1$ Hz, *ortho*-N^+), 8.43 (d, 2H, $J = 8.2$ Hz, *para*-N^+), 7.92 (dd, 2H, *meta*-N^+), 6.80 (m, 4H, *ortho*-O), 6.66 (m, 4H, *meta*-O), 5.63 (s, 4H, CH_2–N^+), 4.49 (q, 4H, $J = 7.1$ Hz, CH_2-α-COO), 4.06 (m, 8H, α-OCH_2), 3.99 (m, 16H, β- and γ-OCH_2), 1.46 (t, 6H, CH_3). HR-ESI-MS: *m/z* [**3b⊂DB24C8**·BF_4]$^+$ calc.: 865.3706, found: 865.3678.

[3b⊂Dinaphtho-24-crown-8][BF_4]$_2$. ^{1}H NMR (CD_3CN): δ (ppm) 9.72 (s, 2H, *ortho*-N^+ and *ortho*-COOEt), 9.33 (d, 2H, $J =$ 6.1 Hz, *ortho*-N^+), 8.15 (d, 2H, $J = 8.1$ Hz, *para*-N^+), 7.92 (dd, 2H, *meta*-N^+), 7.64 (m, 4H, *ortho*-Np), 7.35 (m, 4H, *meta*-Np), 7.00 (s, 4H, *ortho*-O), 5.66 (s, 4H, CH_2–N^+), 4.27 (q, 4H, $J =$ 7.1 Hz, CH_2-α-COO), 4.12 (m, 8H, α-OCH_2), 4.09 (m, 8H, γ-OCH_2), 4.05 (m, 8H, β-OCH_2), 1.24 (t, 6H, CH_3). HR-ESI-MS: *m/z* [**3b⊂DN24C8**·BF_4]$^+$ calc.: 965.4019, found: 965.4057.

[4⊂24-Crown-8][BF_4]$_2$. ^{1}H NMR (CD_3CN): δ (ppm) 8.98 (d, 4H, $J = 5.8$ Hz, *ortho*-N^+), 8.60 (t, 2H, $J = 7.8$ Hz, *para*-N^+), 8.13 (ps-t, 4H, *meta*-N^+), 5.26 (s, 4H, CH_2–N^+), 3.55 (s, 32H, CH_2-crown). HR-ESI-MS: *m/z* [**4⊂24C8**·BF_4]$^+$ calc.: 625.3283, found: 625.3283.

[4⊂Dibenzo-24-crown-8][BF_4]$_2$. ^{1}H NMR (CD_3CN): δ (ppm) 8.92 (d, 4H, $J = 5.8$ Hz, *ortho*-N^+), 8.19 (t, 2H, $J = 7.6$ Hz, *para*-N^+), 7.80 (m, 4H, *meta*-N^+), 6.87 (m, 8H, *ortho*- and *meta*-O), 5.34 (s, 4H, CH_2–N^+), 4.07 (m, 8H, α-OCH_2), 3.82 (m, 8H, β-OCH_2) 3.73 (m, 8H, γ-OCH_2). HR-ESI-MS: *m/z* [**4⊂DB24C8**·BF_4]$^+$ calc.: 721.3283, found: 721.3300.

[4⊂Dinaphtho-24-crown-8][BF_4]$_2$. ^{1}H NMR (CD_3CN): δ (ppm) 8.94 (d, 4H, $J = 5.8$ Hz, *ortho*-N^+), 8.27 (t, 2H, $J =$ 7.6 Hz, *para*-N^+), 7.90 (*ps*-t, 4H, *meta*-N^+), 7.67 (m, 4H, *ortho*-Np), 7.31 (m, 4H, *meta*-Np), 7.19 (s, 4H, *ortho*-O), 5.27 (s, 4H, CH_2–N^+), 4.20 (m, 8H, α-OCH_2), 3.90 (m, 8H, β-OCH_2), 3.78 (s, 8H, γ-OCH_2). HR-ESI-MS: *m/z* [**4⊂DN24C8**·BF_4]$^+$ calc.: 821.3596, found: 821.3564.

[5a⊂24-Crown-8][BF_4]$_2$. ^{1}H NMR (CD_3CN): δ (ppm) 8.73 (d, 4H, $J = 6.5$ Hz, *ortho*-N^+), 7.89 (d, 4H, *meta*-N^+), 5.14 (s, 4H, CH_2–N^+), 3.57 (s, 32H, CH_2-crown), 2.68 (s, 6H, CH_3). HR-ESI-MS: *m/z* [**5a⊂24C8**·BF_4]$^+$ calc.: 653.3596, found: 653.3593.

[5a⊂Dibenzo-24-crown-8][BF_4]$_2$. ^{1}H NMR (CD_3CN): δ (ppm) 8.73 (d, 4H, $J = 6.1$ Hz, *ortho*-N^+), 7.52 (broad, 4H, *meta*-N^+), 6.88 (m, 8H, *ortho*- and *meta*-O), 5.26 (s, 4H, CH_2–N^+), 4.08 (m, 8H, α-OCH_2), 3.81 (m, 8H, β-OCH_2), 3.71 (m, 8H, γ-OCH_2), 2.32 (s, 6H, CH_3). HR-ESI-MS: *m/z* [**5a⊂DB24C8**·BF_4]$^+$ calc.: 749.3596, found: 749.3597.

[5a⊂Dinaphtho-24-crown-8][BF_4]$_2$. ^{1}H NMR (CD_3CN): δ (ppm) 8.73 (d, 4H, $J = 6.1$ Hz, *ortho*-N^+), 7.56 (broad, 4H, *meta*-N^+), 7.67 (m, 4H, *ortho*-Np), 7.32 (m, 4H, *meta*-Np), 7.17 (s, 4H, *ortho*-O), 5.22 (s, 4H, CH_2–N^+), 4.19 (m, 8H, α-OCH_2), 3.92 (m, 8H, β-OCH_2), 3.82 (s, 8H, γ-OCH_2), 2.13 (s, 6H, CH_3). HR-ESI-MS: *m/z* [**5a⊂DN24C8**·BF_4]$^+$ calc.: 849.3909, found: 849.3903.

[5b⊂24-Crown-8][BF_4]$_2$. ^{1}H NMR (CD_3CN): δ (ppm) 8.86 (s, 2H, *ortho*-N^+ and *ortho*-CH_3), 8.74 (d, 2H, $J = 5.8$ Hz, *ortho*-N^+), 8.41 (d, 2H, $J = 8.1$, *para*-N^+), 7.99 (dd, 2H, *meta*-N^+), 5.19 (s, 4H, CH_2–N^+), 3.58 (s, 32H, CH_2-crown), 2.58 (s, 6H, CH_3). HR-ESI-MS: *m/z* [**5b⊂24C8**·BF_4]$^+$ calc.: 653.3596, found: 653.3586.

[5b⊂Dibenzo-24-crown-8][BF_4]$_2$. ^{1}H NMR (CD_3CN): δ (ppm) 8.75 (s, 2H, *ortho*-N^+ and *ortho*-CH_3), 8.68 (broad, 2H, *ortho*-N^+), 8.00 (broad, 2H, *para*-N^+), 7.66 (m, 2H, *meta*-N^+), 6.88 (m, 8H, *ortho*- and *meta*-O), 5.28 (s, 4H, CH_2–N^+), 4.08 (m, 8H, α-OCH_2), 3.81 (m, 8H, β-OCH_2), 3.70 (m, 8H, γ-OCH_2), 2.34 (s, 6H, CH_3). HR-ESI-MS: *m/z* [**5b⊂DB24C8**·BF_4]$^+$ calc.: 749.3596, found: 749.3569.

[5b⊂Dinaphtho-24-crown-8][BF_4]$_2$. ^{1}H NMR (CD_3CN): δ (ppm) 8.78 (s, 2H, *ortho*-N^+ and *ortho*-CH_3), 8.71 (broad, 2H, *ortho*-N^+), 7.96 (broad, 2H, *para*-N^+), 7.64 (m, 2H, *meta*-N^+), 7.67 (m, 4H, *ortho*-Np), 7.31 (m, 4H, *meta*-Np), 7.20 (s, 4H, *ortho*-O), 5.24 (s, 4H, CH_2–N^+), 4.20 (m, 8H, α-OCH_2), 3.90 (m, 8H, β-OCH_2), 3.77 (m, 8H, γ-OCH_2), 2.32 (s, 6H, CH_3). HR-ESI-MS: *m/z* [**5b⊂DN24C8**·BF_4]$^+$ calc.: 849.3909, found: 849.3928.

[6a⊂24-Crown-8][BF_4]$_2$. ^{1}H NMR (CD_3CN): δ (ppm) 8.60 (d, 4H, $J = 7.3$ Hz, *ortho*-N^+), 7.45 (d, 4H, *meta*-N^+), 4.97 (s, 4H, CH_2–N^+), 4.13 (s, 6H, OCH_3), 3.57 (s, 32H, CH_2-crown). HR-ESI-MS: *m/z* [**6a⊂24C8**·BF_4]$^+$ calc.: 685.3495, found: 685.3466.

[6a⊂Dibenzo-24-crown-8][BF_4]$_2$. ^{1}H NMR (CD_3CN): δ (ppm) 8.62 (broad, 4H, *ortho*-N^+), 7.10 (broad, 4H, *meta*-N^+), 6.90 (m, 8H, *ortho*- and *meta*-O), 5.11 (s, 4H, CH_2–N^+), 4.09 (m, 8H, α-OCH_2), 3.85 (s, 6H, OCH_3), 3.81 (m, 8H, β-OCH_2), 3.70 (m, 8H, γ-OCH_2). HR-ESI-MS: *m/z* [**6a⊂DB24C8**·BF_4]$^+$ calc.: 781.3495, found: 781.3531.

[6a⊂Dinaphtho-24-crown-8][BF_4]$_2$. ^{1}H NMR (CD_3CN): δ (ppm) 8.59 (broad, 4H, *ortho*-N^+), 7.11 (broad, 4H, *meta*-N^+), 7.68 (m, 4H, *ortho*-Np), 7.34 (m, 4H, *meta*-Np), 7.23 (s, 4H, *ortho*-O), 5.08 (s, 4H, CH_2–N^+), 4.22 (m, 8H, α-OCH_2), 3.91 (m, 8H, β-OCH_2), 4.09 (s, 6H, OCH_3), 3.79 (s, 8H, γ-OCH_2). HR-ESI-MS: *m/z* [**6a⊂DN24C8**·BF_4]$^+$ calc.: 881.3808, found: 881.3797.

[6b⊂24-Crown-8][BF_4]$_2$. ^{1}H NMR (CD_3CN): δ (ppm) 8.74 (s, 2H, *ortho*-N^+ and *ortho*-OCH_3), 8.52 (d, 2H, $J = 5.7$ Hz, *ortho*-N^+), 8.12 (dd, 2H, $J_{m-p} = 8.8$, $J_{o-p} = 2.5$ Hz, *para*-N^+), 8.00 (dd, 2H, *meta*-N^+), 5.21 (s, 4H, CH_2–N^+), 4.16 (s, 6H, OCH_3), 3.58 (s, 32H, CH_2-crown). HR-ESI-MS: *m/z* [**6b⊂24C8**·BF_4]$^+$ calc.: 685.3495, found: 685.3480.

[6b⊂Dibenzo-24-crown-8][BF_4]$_2$. ^{1}H NMR (CD_3CN): δ (ppm) 8.69 (s, 2H, *ortho*-N^+ and *ortho*-OCH_3), 8.47 (broad, 2H, *ortho*-N^+), 7.65 (broad, 4H, *meta*-N^+ and *para*-N^+), 6.88 (m, 8H, *ortho*- and *meta*-O), 5.33 (s, 4H, CH_2–N^+), 4.08 (m, 8H, α-OCH_2), 3.85 (s, 6H, OCH_3), 3.81 (m, 8H, β-OCH_2), 3.71 (m, 8H, γ-OCH_2). HR-ESI-MS: *m/z* [**6b⊂DB24C8**·BF_4]$^+$ calc.: 781.3495, found: 781.3506.

[6b⊂Dinaphtho-24-crown-8][BF_4]$_2$. ^{1}H NMR (CD_3CN): δ (ppm) 8.75 (s, 2H, *ortho*-N^+ and *ortho*-OCH_3), 8.52 (broad, 2H, *ortho*-N^+), 7.66 (broad, 4H, *meta*-N^+ and *para*-N^+), 7.69 (m, 4H, *ortho*-Np), 7.34 (m, 4H, *meta*-Np), 7.20 (s, 4H, *ortho*-O), 5.33 (s, 4H, CH_2–N^+), 4.22 (m, 8H, α-OCH_2), 3.94 (m, 8H, β-OCH_2), 3.80 (m, 14H, γ-OCH_2 + OCH_3). HR-ESI-MS: *m/z* [**6b⊂DN24C8**·BF_4]$^+$ calc.: 881.3808, found: 881.3835.

[7a⊂24-Crown-8][BF_4]$_2$. ^{1}H NMR (CD_3CN): δ (ppm) 7.79 (d, 4H, $J = 7.1$ Hz, *ortho*-N^+), 6.84 (d, 4H, *meta*-N^+), 6.78 (br, 4H, NH_2), 4.51 (s, 4H, CH_2–N^+), 3.57 (s, 32H, CH_2-crown). HR-ESI-MS: *m/z* [**7a⊂24C8**·BF_4]$^+$ not observed.

[7a⊂Dibenzo-24-crown-8][BF_4]$_2$. ^{1}H NMR (CD_3CN): δ (ppm) 7.71 (d, 4H, $J = 7.2$ Hz, *ortho*-N^+), 6.76 (d, 4H, *meta*-N^+), 6.90 (m, 8H, *ortho*- and *meta*-O), 6.70 (broad, 4H, NH_2), 4.46 (s, 4H, CH_2–N^+), 4.08 (m, 8H, α-OCH_2), 3.80 (m, 8H, β-OCH_2), 3.70 (m, 8H, γ-OCH_2). HR-ESI-MS: *m/z* [**7a⊂DB24C8**·BF_4]$^+$ calc.: 751.3501, found: 751.3487.

[7a⊂Dinaphtho-24-crown-8][BF_4]$_2$. ^{1}H NMR (CD_3CN): δ (ppm) 7.67 (d, 4H, $J = 7.3$ Hz, *ortho*-N^+), 6.77 (d, 4H, *meta*-N^+), 7.68 (m, 4H, *ortho*-Np), 7.32 (m, 4H, *meta*-Np), 7.21 (s, 4H, *ortho*-O), 4.36 (s, 4H, CH_2–N^+), 4.23 (m, 8H, α-OCH_2), 3.92 (m, 8H, β-OCH_2), 3.78 (s, 8H, γ-OCH_2). HR-ESI-MS: *m/z* [**7a⊂DN24C8**·BF_4]$^+$ calc.: 851.3814, found: 851.3812.

[7b⊂24-Crown-8][BF_4]$_2$. ^{1}H NMR (CD_3CN): δ (ppm) 8.01 (s, 2H, *ortho*-N^+ and *ortho*-NH_2), 7.84 (broad, 2H, *ortho*-N^+), 7.65 (m, 2H, *para*-N^+), 7.61 (m, 2H, *meta*-N^+), 5.50 (br, 4H, NH_2), 4.93 (s, 4H, CH_2–N^+), 3.55 (s, 32H, CH_2-crown). HR-ESI-MS: *m/z* [**7b⊂24C8**·BF_4]$^+$ calc.: 655.3501, found: 655.3495.

[7b⊂Dibenzo-24-crown-8][BF_4]$_2$. ^{1}H NMR (CD_3CN): δ (ppm) 7.87 (s, 2H, *ortho*-N^+ and *ortho*-NH_2), 7.73 (broad, 2H, *ortho*-N^+), 7.50 (m, 2H, *para*-N^+), 7.47 (m, 2H, *meta*-N^+), 6.90 (m, 8H, *ortho*- and *meta*-O), 5.40 (broad, 4H, NH_2), 4.90 (s, 4H, CH_2–N^+), 4.08 (m, 8H, α-OCH_2), 3.80 (m, 8H, β-OCH_2), 3.70 (m, 8H, γ-OCH_2). HR-ESI-MS: *m/z* [**7b⊂DB24C8**·BF_4]$^+$ calc.: 751.3501, found: 751.3492.

[7b⊂Dinaphtho-24-crown-8][BF_4]$_2$. ^{1}H NMR (CD_3CN): δ (ppm) 7.94 (s, 2H, *ortho*-N^+ and *ortho*-NH_2), 7.73 (broad, 2H, *ortho*-N^+), 7.46 (m, 2H, *para*-N^+), 7.44 (m, 2H, *meta*-N^+), 7.38 (m, 4H, *ortho*-Np), 7.32 (m, 4H, *meta*-Np), 7.23 (s, 4H, *ortho*-O), 4.88 (s, 4H, CH_2–N^+), 4.23 (m, 8H, α-OCH_2), 3.91 (m, 8H, β-OCH_2), 3.77 (s, 8H, γ-OCH_2). HR-ESI-MS: *m/z* [**7b⊂DN24C8**·BF_4]$^+$ calc.: 851.3814, found: 851.3799.

[9⊂24-Crown-8][BF_4]$_4$. ^{1}H NMR (CD_3CN): δ (ppm) 9.32 (d, 4H, $J = 6.3$ Hz, *ortho*-N^+–Et), 9.04 (d, 4H, $J = 6.8$ Hz, *ortho*-N^+–Bn), 8.54 (d, 4H, *meta*-N^+–Et), 8.48 (d, 4H, *meta*-N^+–Bn), 7.55 (m, 10H, *ortho*-, *meta*- and *para*-Ph), 5.88 (s, 4H, Bn), 5.44 (s, 4H, CH_2–N^+), 3.52 (s, 32H, CH_2-crown). HR-ESI-MS: *m/z* [**9⊂24C8**·$(BF_4)_2$]$^{2+}$ calc.: 524.2470, found: 524.2455.

[9⊂Dibenzo-24-crown-8][BF_4]$_4$. ^{1}H NMR (CD_3CN): δ (ppm) 9.32 (d, 4H, $J = 6.3$ Hz, *ortho*-N^+–Et), 8.96 (d, 4H, $J = 6.8$ Hz, *ortho*-N^+–Bn), 8.16 (d, 4H, *meta*-N^+–Et), 8.11 (d, 4H, *meta*-N^+–Bn), 7.56 (m, 10H, *ortho*-, *meta*- and *para*-Ph), 6.64 (m, 4H, *ortho*-O), 6.44 (m, 4H, *meta*-O), 5.86 (s, 4H, Bn), 5.62 (s, 4H, CH_2–N^+), 4.04 (broad, 8H, α-OCH_2), 4.03 (broad, 8H, β-OCH_2), 4.01 (broad, 8H, γ-OCH_2). HR-ESI-MS: *m/z* [**9⊂DB24C8**·$(BF_4)_2$]$^{2+}$ calc.: 572.2470, found: 572.2479.

[9⊂Dinaphtho-24-crown-8][BF_4]$_4$. ^{1}H NMR (CD_3CN): δ (ppm) 9.33 (d, 4H, $J = 6.3$ Hz, *ortho*-N^+–Et), 8.57 (d, 4H, $J = 6.8$ Hz, *ortho*-N^+–Bn), 8.17 (d, 4H, *meta*-N^+–Et), 7.67 (d, 4H, *meta*-N^+–Bn), 7.33 (broad, 4H, *ortho*-crown), 7.00 (s, 4H, *ortho*-O-crown), 6.93 (broad, 4H, *meta*-crown), 5.69 (s, 4H, Bn), 5.67 (s, 4H, CH_2–N^+), 4.20 (broad, 8H, α-OCH_2), 4.16 (broad, 8H, β-OCH_2), 4.12 (broad, 8H, γ-OCH_2). HR-ESI-MS: *m/z* [**9⊂DN24C8**·$(BF_4)_2$]$^{2+}$ calc.: 622.2626, found: 622.2619.

Table 5 Crystal data, solution and refinement parameters for single crystal structure determinations

Compound	[**1⊂DB24C8**][BF_4]$_2$	[**1⊂DN24C8**][BF_4]$_2$	[**2a⊂DB24C8**][BF_4]$_2$	[**2a⊂DN24C8**][BF_4]$_2$	[**3a⊂DB24C8**][BF_4]$_2$	[**3b⊂DB24C8**][BF_4]$_2$	[**6b⊂24C8**][BF_4]$_2$	[**4⊂24C8**][BF_4]$_2$	[**9⊂DN24C8**][BF_4]$_4$
CCDC number	286500	286501	286502	286503	286504	286505	286506	286507	286508
Formula	$C_{48}H_{58}B_2F_8N_6O_{12}$	$C_{56}H_{62}B_2F_8N_6O_{12}$	$C_{50}H_{46}B_2F_8N_4O_{12}$	$C_{58}H_{64}B_2F_8N_4O_{12}$	$C_{46}H_{60}B_2F_8N_4O_{12}$	$C_{44}H_{60}B_2F_8N_4O_{16}$	$C_{30}H_{50}B_2F_8N_2O_{10}$	$C_{28}H_{46}B_2F_8N_2O_8$	$C_{76}H_{82}B_4F_{16}N_8O_9$
Formula weight	1084.62	1184.74	1082.64	1182.75	1034.60	1074.58	772.34	712.29	1598.74
Crystal system	Monoclinic	Monoclinic	Triclinic	Monoclinic	Orthorhombic	Orthorhombic	Monoclinic	Monoclinic	Triclinic
Space group	$P2_1/c$ (no. 14)	$P2_1/n$ (no. 14)	$P\bar{1}$ (no. 2)	Pn (no. 7)	$P2_1/c$ (no. 14)	*Pbca* (no. 61)	$P2_1$ (no. 4)	$P2_1/c$ (no. 14)	$P\bar{1}$ (no. 2)
T/K	293(2)	293(2)	293(2)	293(2)	293(2)	293(2)	293(2)	173.0(5)	173.0(5)
a/Å	10.5068(3)	12.2482(7)	11.6700(9)	12.3959(8)	13.2421(4)	9.3357(1)	10.4924(6)	17.433(5)	13.598(2)
b/Å	12.0843(3)	37.030(2)	13.1966(10)	19.1294(12)	15.7037(5)	22.4319(3)	16.5364(10)	20.012(5)	16.807(3)
c/Å	21.5489(7)	13.0751(7)	17.1182(13)	12.9148(8)	12.1739(4)	25.0932(2)	10.7738(6)	19.631(5)	17.859(3)
α/°			91.475(2)						87.625(3)
β/°	102.703(1)	111.498(2)	96.658(2)	112.855(1)	94.909(1)		96.584(1)	93.572(4)	70.059(2)
γ/°			91.858(2)						
V/Å^3	2669.0(1)	5517.7(5)	2616.0(3)	2822.0(3)	2522.3(1)	5255.0(1)	1857.0(2)	6836(3)	3831.2(11)
Z	2	4	2	2	2	4	2	8	2
ρ/g cm^{-3}	1.350	1.426	1.374	1.392	1.362	1.174	1.381	1.384	1.386
μ/mm^{-1}	0.114	0.117	0.115	0.113	0.116	0.103	0.126	0.126	0.116
Reflections used	4624	5635	9196	9879	4399	2440	6537	7150	13433
Variables	343	757	685	747	354	361	469	865	1022
R_1 [$I > 2\sigma(I)$][a]	0.0824	0.1121	0.0713	0.0964	0.0940	0.1300	0.0784	0.0781	0.1055
R_1 (all data)	0.1768	0.1529	0.0938	0.1299	0.1625	0.1648	0.0865	0.1486	0.1090
R_2w [$I > 2\sigma(I)$][b]	0.2100	0.2105	0.1957	0.2107	0.2672	0.2637	0.2171	0.1802	0.2979
R_2w (all data)	0.2529	0.2335	0.2168	0.2264	0.3025				
GoF on F^2	0.939	1.157	1.039	1.132	1.045	0.2961	0.2263	0.2225	0.3620
						1.329	1.036	1.028	1.125

[a] $R_1 = \Sigma \mid |F_o| - |F_c| \mid / \Sigma |F_o|$. [b] $R_2w = [\Sigma [w(F_o^2 - F_c^2)^2] / \Sigma [w(F_o^2)^2]]^{1/2}$, where $w = q[\sigma^2(F_o^2) + (aP)^2 + bP]^{-1}$.

General procedure for the K_a measurements

A ^{1}H NMR spectrum of an equimolar solution (2.0×10^{-3} M) of the 1,2-bis(pyridinium)ethane salt and 24-crown-8 ether in CD_3CN was recorded at 25 °C. The concentration of all the species at equilibrium was determined using the initial crown and thread concentrations and the integration of the ethane resonance of free and complexed species. For pseudorotaxanes in fast exchange, association constants were determined by titrating a solution (2.0×10^{-3} M) of the 1,2-bis(pyridinium)ethane salt in CD_3CN with increasing amounts of a solution (0.2 M in $CDCl_3$) of crown ether until saturation was indicated (for these results see ESI†). The change in chemical shift of the ethane resonance was fitted using a non-linear least-squares model using the software WinEQNMR.[21]

X-Ray crystal structure determination

Crystals were mounted on a short glass fiber attached to a tapered copper pin. A full hemisphere of data was collected with 30 s frames on a Brüker APEX diffractometer fitted with a CCD-based detector using Mo-Kα radiation ($\lambda = 0.71073$ Å). Decay (<1%) was monitored by 50 standard data frames measured at the beginning and end of data collections. Diffraction data and unit-cell parameters were consistent with the assigned space groups. Lorentzian polarization corrections and empirical absorption corrections, based on redundant data at varying effective azimuthal angles, were applied to the data set. The structure was solved by direct methods, completed by subsequent Fourier syntheses and refined with full-matrix least-squares methods against $|F^2|$ data. All non-hydrogen atoms were refined anisotropically. All hydrogen atoms were treated as idealized contributions. Scattering factors and anomalous dispersion coefficients are contained in the SHELXTL 5.03 program library.[33] Crystal data collection, solution and structure refinement parameters are listed in Table 5.

CCDC reference numbers 286500–286508.

For crystallographic data in CIF or other electronic format see DOI: 10.1039/b514528g

Acknowledgements

The authors thank NSERC of Canada for providing funds in the form of a Discovery Grant to S. J. L.

References

1 D. A. Leigh, A. Murphy, J. P. Smart and A. M. Z. Slawin, *Angew. Chem., Int. Ed. Engl.*, 1997, **36**, 728–732; A. G. Johnston, D. A. Leigh, R. J. Pritchard and M. D. Deegan, *Angew. Chem., Int. Ed. Engl.*, 1995, **34**, 1209–1212; J. A. Wisner, P. D. Beer, M. G. B. Drew and M. R. Sambrook, *J. Am. Chem. Soc.*, 2002, **124**, 12 469–12 476; G. Kaiser, T. Jarrosson, S. Otto, Y.-F. Ng, A. D. Bond and J. K. M. Sanders, *Angew. Chem., Int. Ed.*, 2004, **43**, 1959–1962; R. Jager and F. Vögtle, *Angew. Chem., Int. Ed. Engl.*, 1997, **36**, 930–944; F. Vögtle, T. Duennwald and T. Schmidt, *Acc. Chem. Res.*, 1996, **29**, 451–460; F. Vögtle, S. Meier and R. Hoss, *Angew. Chem., Int. Ed. Engl.*, 1992, **31**, 1619–1622; R. S. Wylie and D. H. Macartney, *J. Am. Chem. Soc.*, 1992, **114**, 3136–3138; H. Ogino, *J. Am. Chem. Soc.*, 1981, **103**, 1303–1304; K. Kim, *Chem. Soc. Rev.*, 2002, **31**, 96–107; C. A. Hunter, *J. Am. Chem. Soc.*, 1992, **114**, 5303–5311; J.-P. Collin, C. Dietrich-Buchecker, P. Gaviña, M. C. Jimenez-Molero and J.-P. Sauvage, *Acc. Chem. Res.*, 2001, **34**, 477–487; P. R. Ashton, P. J. Campbell, E. J. T. Chrystal, P. T. Glinke, S. Menzer, D. Philp, N. Spencer, J. F. Stoddart, P. A. Tasker and D. J. Williams, *Angew. Chem., Int. Ed. Engl.*, 1995, **34**, 1865–1869; S. A. Nepogodiev and J. F. Stoddart, *Chem. Rev.*, 1998, **98**, 1959–1976; J. O. Jeppesen, J. Perkins, J. Becher and J. F. Stoddart, *Org. Lett.*, 2000, **2**, 3547–3550; P. L. Anelli, P. R. Ashton, R. Ballardini, V. Balzani, M. Delgado, M. T. Gandolfi, T. T. Goodnow, A. E. Kaifer, D. Philp, M. Pietraszkiewicz, L. Prodi, M. V. Reddington, A. M. Z. Slawin, N. Spencer, J. F. Stoddart, C. Vicent and D. J. Williams, *J. Am. Chem. Soc.*, 1992, **114**, 193–218.

2 S. J. Loeb and D. A. Tramontozzi, *Org. Biomol. Chem.*, 2005, **3**, 1393–1401; S. J. Cantrill, D. A. Fulton, A. M. Heiss, A. R. Pease, J. F. Stoddart, A. J. P. White and D. J. Williams, *Chem.–Eur. J.*, 2000, **6**, 2274–2287; J. Cao, M. C. T. Fyfe, J. F. Stoddart, G. R. L. Cousins and P. T. Glink, *J. Org. Chem.*, 2000, **65**, 1937–1946; S. J. Rowan, S. J. Cantrill and J. F. Stoddart, *Org. Lett.*, 1999, **1**, 129–132.

3 *Molecular Catenanes, Rotaxanes and Knots*, J.-P. Sauvage and C. Dietrich-Buchecker, eds., VCH-Wiley, Weinheim, 1999.

4 M. R. Sambrook, P. D. Beer, J. A. Wisner, R. L. Paul, A. R. Cowley, F. Szemesa and M. B. G. Drew, *J. Am. Chem. Soc.*, 2005, **127**, 2292–2302; D. A. Leigh, M. A. F. Morales, E. M. Perez, J. K. Y. Wong, C. G. Saiz, A. M. Z. Slawin, A. J. Carmichael, D. M. Haddleton, A. M. Brouwer, W. J. Buma, G. W. H. Wurpel, S. Leon and F. Zerbetto, *Angew. Chem., Int. Ed.*, 2005, **44**, 3062–3067; Y. Liu, P. A. Bonvallet, S. A. Vignon, S. I. Khan and J. F. Stoddart, *Angew. Chem., Int. Ed.*, 2005, **44**, 3050–3055; C. A. Schalley, W. Reckien, S. Peyerimhoff, B. Baytekin and F. Vögtle, *Chem.–Eur. J.*, 2004, **10**, 4777–4789; S. A. Vignon, T. Jarrosson, T. Iijima, H.-R. Tseng, J. K. M. Sanders and J. F. Stoddart, *J. Am. Chem. Soc.*, 2004, **126**, 9884–9885.

5 For some recent examples of molecular machines and devices, see: Y. Liu, A. H. Flood, P. A. Bonvallet, S. A. Vignon, B. H. Northrop, H.-R. Tseng, J. O. Jeppesen, T. J. Huang, B. Brough, M. Baller, S. Magonov, S. D. Solares, W. A. Goddard, C.-M. Ho and J. F. Stoddart, *J. Am. Chem. Soc.*, 2005, **127**, 9745–9759; J.-P. Sauvage, *Chem. Commun.*, 2005, 1507–1510; J. D. Badjic, V. Balzani, A. Credi, S. Silvi and J. F. Stoddart, *Science*, 2004, **303**, 1845–1849; R. Hernandez, H.-R. Tseng, J. W. Wong, J. F. Stoddart and J. I. Zink, *J. Am. Chem. Soc.*, 2004, **126**, 3370–3371; W. S. Jeon, E. Kim, Y. H. Ko, I. Hwang, J. W. Lee, S.-Y. Kim, H.-J. Kim and K. Kim, *Angew. Chem., Int. Ed.*, 2004, **44**, 87–91; J. V. Hernández, E. R. Kay and D. A. Leigh, *Science*, 2004, **306**, 1532–1537; D. A. Leigh, J. K. Y. Wong, F. Dehez and F. Zerbetto, *Nature*, 2003, **424**, 174–179; 'Molecular Machines Special Issue' *Acc. Chem. Res.*, 2001, **34**, 409–522.

6 S. J. Loeb and J. A. Wisner, *Angew. Chem., Int. Ed.*, 1998, **37**, 2838–2840.

7 B. L. Allwood, N. Spencer, H. Shahriari-Zavareh, J. F. Stoddart and D. J. Williams, *J. Chem. Soc., Chem. Commun.*, 1987, 1064–1066 [BPP34C10 is bis(paraphenylene)-34-crown-10].

8 S. J. Cantrill, A. R. Pease and J. F. Stoddart, *J. Chem. Soc., Dalton Trans.*, 2000, 3715–3734; P. T. Glink, C. Schiavo, J. F. Stoddart and D. J. Williams, *Chem. Commun.*, 1996, 1483–1490.

9 N. Georges, S. J. Loeb, J. Tiburcio and J. A. Wisner, *Org. Biomol. Chem.*, 2004, **2**, 2751–2756; G. J. E. Davidson, S. J. Loeb, N. A. Parekh and J. A. Wisner, *J. Chem. Soc., Dalton Trans.*, 2001, 3135–3136; S. J. Loeb and J. A. Wisner, *Chem. Commun.*, 2000, 845–846; S. J. Loeb and J. A. Wisner, *Chem. Commun.*, 1998, 2757–2758.

10 A. L. Hubbard, G. J. E. Davidson, R. H. Patel, J. A. Wisner and S. J. Loeb, *Chem. Commun.*, 2004, 138–139.

11 S. J. Loeb and J. A. Wisner, *Chem. Commun.*, 2000, 1939–1940.

12 G. J. E. Davidson, Ph.D. Dissertation, University of Windsor, Canada, 2004.

13 S. J. Loeb, *Chem. Commun.*, 2005, 1511–1518; D. J. Hoffart and S. J. Loeb, *Angew. Chem., Int. Ed.*, 2005, **44**, 901–904; G. J. E. Davidson and S. J. Loeb, *Angew. Chem., Int. Ed.*, 2003, **42**, 74–77; J. Tiburcio, G. J. E. Davidson and S. J. Loeb, *Chem. Commun.*, 2002, 1282–1283.

14 M. I. Attalla, N. S. McAlpine and L. A. Summers, *Z. Naturforsch., B*, 1984, **39**, 74–78.

15 F. Huang, J. W. Jones, C. Slebodnick and H. W. Gibson, *J. Am. Chem. Soc.*, 2003, **125**, 14 458–14 464; J. W. Jones and H. W. Gibson, *J. Am. Chem. Soc.*, 2003, **125**, 7001–7004.

16 For a discussion about the role of *tert*-butyl groups as stoppers, see: Y. Tachibana, N. Kihara, Y. Furusho and T. Takata, *Org. Lett.*, 2004, **6**, 4507–4509; P. R. Ashton, I. Baxter, M. C. T. Fyfe, F. M. Raymo, N. Spencer, J. F. Stoddart, A. J. P. White and D. J. Williams, *J. Am. Chem. Soc.*, 1998, **120**, 2297–2307.

17 C. L. Perrin and T. J. Dwyer, *Chem. Rev.*, 1990, **90**, 935–967.

18 M. Venturi, S. Dumas, V. Balzani, J. Cao and J. F. Stoddart, *New J. Chem.*, 2004, **28**, 1032–1037.

19 W. Henderson and J. S. McIndoe, *Mass Spectrometry of Inorganic, Coordination and Organometallic Compounds*, Wiley, Chichester,2005.

20 P. R. Ashton, E. J. T. Chrystal, P. T. Glink, S. Menzer, C. Schiavo, N. Spencer, J. F. Stoddart, P. A. Tasker, A. J. P. White and D. J. Williams, *Chem.–Eur. J.*, 1996, **2**, 709–728; J. C. Adrian and C. S. Wilcox, *J. Am. Chem. Soc.*, 1991, **113**, 678–680.
21 M. J. Hynes, *J. Chem. Soc., Dalton Trans.*, 1993, 311–312.
22 B. J. Coe, J. A. Harris, I. Asselberghs, K. Wostyn, K. Clays, A. Persoons, B. S. Brunschwig, S. J. Coles, T. Gelbrich, M. E. Light, M. B. Hursthouse and K. Nakatani, *Adv. Funct. Mater.*, 2003, **13**, 347–357; M. J. Smith, W. Clegg, K. A. Nguyen, J. E. Rogers, R. Pachter, P. A. Fleitz and H. L. Anderson, *Chem. Commun.*, 2005, 2433–2435.
23 P. R. Ashton, M. C. T. Fyfe, S. K. Hickingbottom, J. F. Stoddart, A. J. P. White and D. J. Williams, *J. Chem. Soc., Perkin Trans. 2*, 1998, 2117–2128.
24 P. R. Ashton, R. A. Bartsch, S. J. Cantrill, R. E. Hanes, Jr., S. K. Hickingbottom, J. N. Lowe, J. A. Preece, J. F. Stoddart, V. S. Talanov and Z.-H. Wang, *Tetrahedron Lett.*, 1999, **40**, 3661–3664.
25 C. Hansch, A. Leo and R. W. Taft, *Chem. Rev.*, 1991, **91**, 165–195.
26 J. R. Horn, D. Russell, E. A. Lewis and K. P. Murphy, *Biochemistry*, 2001, **40**, 1774–1778; J. R. Horn, J. F. Brandts and K. P. Murphy, *Biochemistry*, 2002, **41**, 7501–7507; D. B. Smithrud, T. B. Wyman and F. Diederich, *J. Am. Chem. Soc.*, 1991, **113**, 5420–5426.
27 D. A. Stauffer, R. E. Barrans, Jr. and D. A. Dougherty, *J. Org. Chem.*, 1990, **55**, 2762–2767.
28 (*a*) P. D. Ross and S. Subramanian, *Biochemistry*, 1981, **20**, 3096–3102; (*b*) Y. Inoue and T. Hakushi, *J. Chem. Soc., Perkin Trans. 2*, 1985, 935–946; (*c*) Z.-P. Yi, H.-L. Chen, Z.-Z. Huang, Q. Huang and J.-S. Yu, *J. Chem. Soc., Perkin Trans. 2*, 2000, 121–127; (*d*) Y. Inoue, T. Hakushi, Y. Liu, L.-H. Tong, B.-J. Shen and D.-S. Jin, *J. Am. Chem. Soc.*, 1993, **115**, 475–481; (*e*) Y. Inoue, Y. Liu, L.-H. Tong, B.-J. Shen and D.-S. Jin, *J. Am. Chem. Soc.*, 1993, **115**, 10 637–10 644.
29 DIAMOND 3.0 – Visual Crystal Structure Information System, CRYSTAL IMPACT, Postfach 1251, D-53002 Bonn, Germany, 2004.
30 G. R. Desiraju, *Chem. Commun.*, 2005, 2995–3001; G. R. Desiraju, *Acc. Chem. Res.*, 1996, **29**, 441–449; G. R. Desiraju, *Acc. Chem. Res.*, 1991, **24**, 290–296.
31 C. A. Hunter and J. K. M. Sanders, *J. Am. Chem. Soc.*, 1990, **112**, 5525–5534; C. A. Hunter, K. R. Lawson, J. Perkins and C. J. Urch, *J. Chem. Soc., Perkin Trans. 2*, 2001, 651–669.
32 G. J. E. Davidson and S. J. Loeb, *Dalton Trans.*, 2003, 4319–4323.
33 G. M. Sheldrick, SHELXTL 6.14 Program Library, Brüker Analytical Instrument Division, Madison, Wisconsin, USA, 2003.

